Novel distributed beamforming algorithms for heterogeneous space terrestrial integrated network

Novel distributed beamforming algorithms for heterogeneous space terrestrial integrated network

Xiaoyan Shi, Rongke Liu *Senior Member, IEEE*, and John S. Thompson *Fellow, IEEE*

***Abstract*—An integrated space-terrestrial network based on the ultra-dense low-earth-orbit (LEO) satellite constellations has been envisioned in both 5G and beyond 5G (B5G) networks. This approach is a powerful solution to some key challenges from Internet-of-Thing (IoT) services, such as the lack of link capacity to deal with large data transfer or coverage in the remote areas. This paper focuses on the beamforming design for the transmissions from multiple LEO satellites, equipped with massive phased array antenna, to a large number of heterogeneous terrestrial terminals. Superposition coding based beamforming is efficient in dealing with the receiver heterogeneity, but at the cost of higher computational complexity. Based on the dual decomposition theory as well as deep-neural-networks (DNNs), this paper proposes to combine the non-linear approximation ability of DNNs with distributed algorithms. This combination not only supports advanced non-orthogonal beamforming algorithms for achieving superior throughput performance, but also keeps the overall computational complexity low and enables the beamforming process to be speed up dramatically through parallel computing.**

***Index Terms*—LEO satellites, beamforming, receiver heterogeneity, distributed algorithms**

I. INTRODUCTION

Recent plans and actions of deploying very large low earth orbit (LEO) satellite constellations such as SpaceX and OneWeb [1], [2], have proven that the ultra-dense LEO satellite network is not only a realizable concept but also an economic one. Orbiting the earth at an altitude from 500 km to 2000 km, LEO satellites provide communication with both vast coverage and low latency. Through interconnecting neighbouring satellites with free space optical links [3], the ultra-dense LEO satellite network establishes global connections with a surprisingly low latency. Reference [4] shows this approach remains competitive against optical fibre in the short range and becomes superior to the terrestrial networks over distances larger than 3000 km.

Benefiting from these powerful features, the LEO satellite network serves as a promising way of complementing the terrestrial networks to address some key challenges coming from the Internet of Things (IoTs) [6]. One area is the provision of internet connection to place where the price of deploying terrestrial infrastructure is prohibitively high. For example, in the monitoring and management related applications in rural areas, oceans or other remote terrains, the collected data is first uploaded to the satellites and then relayed to the core network [10]–[12]. This paradigm is described in [13] as the Internet of Remote Things. The other use case involves offloading the IoT traffic from the congested terrestrial networks which are usually densely deployed. In this case, the satellite serves essentially as the high bandwidth backhaul links [14]. LEO satellite networks offer promising solutions to the latency and capacity requirements from these applications. For example as studied in [4], [12] the LEO satellite network can satisfy the stringent latency requirement of implementing the wide-area situational awareness in the smart grid. Recent works [7]–[9] demonstrate the adoption of the massive-MIMO (M-MIMO) technique at the LEO satellite as one of the key techniques that enable large system capacity to support rate hungry services, such as the massive uploading of the sensor data, the proactive caching of high-quality videos at the cellular base stations or the augmented reality services [15], [16].

In this paper, we study the use of massive phased array antennas at the LEO satellites to deliver Quality of Service (QoS) guaranteed transmissions to a large number of outdoor heterogeneous terrestrial terminals. The majority of the LEO satellite receivers are located outdoors due to large path loss from the satellite-ground channel. For example, in SpaceX [2], its operating system is primarily designed for line-of-sight (LOS) propagation. Without loss of generality, we consider two classes of users, differentiated by their receiving capabilities. One typical application of LEO satellites is to supplement terrestrial backhaul links [14]. In this case, the ground users of the satellites are 5G access points with directional antennas. In the cases of typical IoT services, such as fetching the sensor data to a private user directly through the satellite-to-ground link [6], low cost receivers with a smaller antenna aperture are more likely to be used.

The goal of this paper is to fully unlock the spatial multiplexing gain inherent to M-MIMO and at the same time avoid the performance degradation due to the use of beamforming in the highly ill-conditioned channels. This paper studies the combination of beamforming and superposition coding, or in a broader term, non-orthogonal multiple access (NOMA), which superimposes the stronger and the weaker users' signal in the power domain and employs successive interference cancellations (SICs) in 5G backhaul link receivers to separate their information from the IoT transmissions. We formulate the beamforming problem under the framework of a QoS constrained optimization so as to provide a mechanism to deal with services with different QoS requests, which is crucial for some latency-sensitive IoT applications.

Applying NOMA in the downlink transmission means that the stronger ground terminal gets extra more information from the satellite than the weaker one. Thus the stronger terminal

Xiaoyan Shi is with both University of Edinburgh and Beihang University (email: Xiaoyan.Shi@ed.ac.uk), John S. Thompson is with University of Edinburgh (email: John.Thompson@ed.ac.uk, Rongke Liu is with Beihang University (email: Rongke_Liu@buaa.edu.cn). This work was supported by the National Key R&D Program of China (Grant No.2020YFB1807102).

may serve as a relay, passing data through terrestrial links to the weaker one. Such cooperation between the satellite and terrestrial wireless links requires cross-layer management such as joint optimization over resource management in the wireless access network and flow control in backhaul links [5]. We present in this paper that the QoS constrained non-orthogonal beamforming problem serves as an essential building block for the cross layer optimization in the space-terrestrial integrated network as envisioned in [6], [14].

To cater for the heterogeneous receivers in M-MIMO communications, the combination between transmit beamforming with superposition coding [17] or in another term MIMO NOMA [18], has been studied extensively in cellular networks [18]–[22]. In the area of LEO satellite communications, some recent works have only considered M-MIMO but without NOMA. In [8] and [9], assuming uniform receiving capability among the ground terminals, downlink beamforming is optimized such that signal-to-leakage-plus-noise ratio (SLNR) is maximized. The solutions to the optimization can be written in closed-form terms. However, once the receiver heterogeneity and the QoS constraints are taken into account, no analytic solution exists anymore and iterative algorithms with high complexity are needed. This paper also differs from [8] and [9] in that these works focus on dealing with challenges of channel estimation brought by user mobility, while we assume all ground terminals to have fixed locations and focus on the design of beamforming algorithm to deal with receiver heterogeneity.

One significant difference between M-MIMO applied to cellular and satellite networks is that the number of radio frequency (RF) chains is much higher in the satellite phased array antenna, resulting in high computational complexity, e.g. the phased array antenna for the LEO satellite proposed in [23] contains 221 RF chains whereas in studies for terrestrial networks [19]–[22], the number is seldomly more than 10 or 20. In cellular networks, zero-forcing or block diagonalization is typically applied in digital beamformings without severely compromising the performance due to channel sparsity, as studied in [20]–[22]. However, this is not the case in LEO satellite communications, where the high correlations between neighboring users make zero-forcing dramatically degrade the performance. This second issue prevents the use of channel diagonalization in satellite communications with a massive number of heterogeneous users to lower the high computational burden such as in [17].

Field-programmable gate arrays (FPGAs) and graphics processing unit (GPU) provide superior distributed computing ability, both of which serve as important ways to boost the onboard processing power as pointed out by the European Space Agency (ESA) roadmaps [31]. To exploit the great potential of distributed computation for solving the NOMA based beamforming problem, we propose novel iterative distributed algorithms based on dual relaxation techniques and the augmented Lagrangian method [30]. To further lower the per iteration complexity of the distributed algorithm, we further resort to the outstanding nonlinear approximation ability of the deep neural networks (DNNs) [38]–[40]. Unlike most of the predecessor DNN related works in beamforming, which directly output the beamformers from the trained DNNs, we use DNNs to approximate the solutions to the subproblem at each iteration of the distributed algorithm. The novel contributions of this paper are introduced as follows:

1) Considering the receiver heterogeneity of the terrestrial network, this paper proposes the application of NOMA beamforming in the downlink transmission of the LEO satellites networks, where a massive number of heterogeneous users are served with full frequency reuse. We also propose to use the stronger terrestrial terminal as the data relay for the weaker ones and show that the QoS constrained beamforming problems are essential for the corresponding cross-layer optimization.
2) To solve the NOMA beamforming problems with QoS constraints, this paper designs a novel distributed beamforming algorithm based on dual relaxation and the augmented Lagrangian method. The proposed beamforming algorithm is implemented in a distributed way across the different user pairs. Numerical simulations demonstrate that given the same QoS constraints, the transmission power can be significantly reduced using the proposed NOMA beamforming methd.
3) To further reduce the per iteration computation complexity of the proposed distributed algorithm, we use DNNs to approximate solutions to the convex subproblem for the distributed algorithm. A theoretical proof of convergence for the distributed algorithm using approximate computing techniques is provided. Numerical demonstrations are also presented to confirm our findings.

The structure of this paper is briefed as follows: in Section II, the system model about the multi-antenna satellite downlink communication is introduced. The QoS constrained beamforming optimization with NOMA is formulated. The distributed beamforming algorithm and a novel approximate computing technique are proposed in Section III with detailed theoretical analysis of the optimality and the computational complexity for the proposed schemes. In Section IV, numerical simulations are given to show the significant system performance gain as well as the massive reduction of computational complexity achieved by the proposed distributed NOMA beamforming scheme. Section V draws the conclusions of this paper.

II. System Model and Problem Formulation

In this section we first introduce the multi-antenna channel models, the antenna architecture and the hybrid beamforming for the downlink transmission of LEO satellite communications with heterogeneous ground receivers. We then formulate the cross-layer optimization in the integrated space-terrestrial network as a motivational case for the introduction of the major problem of this paper, the QoS constrained beamforming optimization with NOMA.

A. Channel Models for Multi-LEO Satellites Phased Array Antenna Communications

The hybrid antenna structure allows for a combination of analog beamforming and digital beamforming, realizing a trade-off between the system capacity and the limited hardware

resources [24]. In this paper, each LEO satellite has a hybrid structured phased array antenna with N_s elements and n_r RF chains, such as the one introduced in [25]. At the user end, a planar array antenna with N_u elements and a single RF chain is installed. In our scenario the ground terminal locations and the trajectory of the satellites are fixed with LOS channels available between the satellites and terrestrial receivers. The existence of LOS channels are typically assumed in relevant research works such as [8], [9] since the LEO satellite systems are usually operated under LOS propagation, especially for fixed ground terminals. This indicates that sufficient frequency and time synchronization can be achieved so that the narrow band channel gain between the m^{th} satellite transmitter and the k^{th} ground user is represented as

$$\mathbf{H}_{m,k}^{\text{sat}} = \sum_{l=1}^{L_k} a_{m,k,l}\mathbf{g}_{m,k,l}\mathbf{h}_{m,k,l}^{\text{H}} \overset{\Delta}{\approx} \sum_{l=1}^{L_k} a_{m,k,l}\mathbf{g}_{m,k,l}\mathbf{h}_{m,k}^{\text{H}}, \quad (1)$$

where $a_{m,k,l}$ is the complex channel gain, L_k is the number of total paths and the array response vectors $\mathbf{g}_{m,k,l} \in \mathbb{C}^{N_u}$, $\mathbf{h}_{m,k,l} \in \mathbb{C}^{N_s}$ are related to the angles-of-departure (AoDs) $\boldsymbol{\theta} = (\theta^x, \theta^y)$ and angles-of-arrival (AoAs) $\boldsymbol{\phi} = (\phi^x, \phi^y)$ (θ^x, ϕ^x are the azimuth angles and θ^y, ϕ^y are elevation angles in the earth-centered earth-fixed coordinate system) respectively. The approximation Δ in (1) is due to the long transmission range of satellite channels, resulting in very little difference between AoDs of each paths. The large scale attenuation factor $a_{m,k,l}$ can be expressed as

$$a_{m,k,l} = G_{m,k}^t G_{m,k}^r \sqrt{L_{m,k}/\xi_{m,k}}, L_{m,k} = \frac{\lambda_c}{4\pi d_{m,k}}, \quad (2)$$

where $G_{m,k}^t$ and $G_{m,k}^r$ are the antenna gains of the transmitting and receiving antenna elements respectively, λ_c is the carrier frequency, $d_{m,k}$ is the distance between the transmitter and the receiver, $L_{m,k}$ is the path loss coefficient and $\xi_{m,k}$ is the rain attenuation coefficient. The subscript l is dropped in (2) since the variations of Ls and ξs among different paths are negligible due to the long transmission distance.

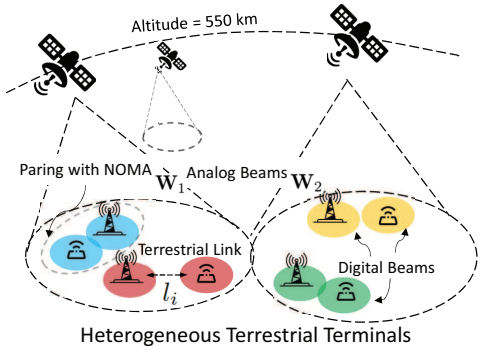

Fig. 1. Heterogeneous LEO Satellite Network with Hybrid Phased Array Antenna.

Based on hybrid beamforming, combine the transmitted signal from all M satellites for user k in $\mathbf{s}_k = [\mathbf{s}_{k1}^{\text{H}}, \cdots, \mathbf{s}_{kM}^{\text{H}}]^{\text{H}} \in \mathbb{C}^{MN_s \times 1}$. Similarly, denote the aggregated analogue and digital beamformer for user k respectively as $\mathbf{W} = \text{Diag}([\mathbf{W}_1, \cdots, \mathbf{W}_M])$ and $\mathbf{d}_k = [\mathbf{d}_{k1}^{\text{H}}, \cdots, \mathbf{d}_{kM}^{\text{H}}]^{\text{H}}$, where $\mathbf{W}_m \in \mathbb{C}^{N_s \times n_r}$ in the block diagonal matrix forms the local analog beamforming codebook at the m^{th} transmitter. The entries of $\mathbf{W}_m$ are the phase shifts with a constant modulus $\frac{1}{\sqrt{N_s}}$. The vector $\mathbf{d}_{km}$ is the digital beamformer at the m^{th} transmitter. Assuming a total number of N_{tot} ground receivers, the whole transmitted signal can be represented as

$$\mathbf{W}\sum_{i}^{N_{\text{tot}}} \mathbf{d}_i x_i = \mathbf{W}\mathbf{D}\mathbf{x}. \quad (3)$$

Denoting $\mathbf{H}_k = \left[\mathbf{H}_{1,k}^{\text{sat}}, \cdots, \mathbf{H}_{M,k}^{\text{sat}}\right]$, the received signal at user k can be expressed as

$$y_k = \mathbf{v}_k^{\text{H}}\mathbf{H}_k\mathbf{W}\left(\mathbf{d}_k x_k + \sum_{i\neq k}^{N_{\text{tot}}} \mathbf{d}_i x_i\right) + z_k, \quad (4)$$

where $\mathbf{v}_k \in \mathbb{C}^{N_u \times 1}$ is the receiver beamformer and $z_k \sim \mathcal{CN}(0, \sigma_k)$ is the complex normally distributed additive receiver noise.

B. Analog Beamforming and Motivational Problems

In this paper, the exact structure of the transmit antenna is based on the one proposed in [23]. The total antenna elements is divided into n_r subarrays, each of which contains $n_{\text{sub}} = N_s/n_r$ antenna elements and is connected to an RF chain. Denote the analog beamformer applied at the l^{th} subarray by $\mathbf{w}_{ml} \in \mathbb{C}^{n_{\text{sub}} \times 1}$. $\mathbf{W}_m$ can be expressed as

$$\mathbf{W}_m = \begin{bmatrix} \mathbf{W}_{m1}, & \mathbf{0}, & \cdots, & \mathbf{0} \\ \mathbf{0}, & \mathbf{W}_{m2}, & \cdots, & \mathbf{0} \\ \vdots, & \vdots, & \ddots, & \vdots \\ \mathbf{0}, & \mathbf{0}, & \cdots, & \mathbf{W}_{mn_r} \end{bmatrix}. \quad (5)$$

Follows the parameter setup in [23], $N_s = n_{\text{sub}} \times n_r = (4 \times 4) \times (21 \times 21)$, indicating that the analog beam formed by the 4×4 analogue subarray is much wider than the digital beam, which is formed by the combination of the 441 analogue subarrays. Therefore, we assume a predetermined $\mathbf{W}_m = \bar{\mathbf{W}}_m$ is applied to illuminate a fixed terrestrial area $\mathcal{A}_m$, where the majority of the terrestrial receivers are based.

The Rician fading model has been widely accepted in the literature for modeling the LOS satellite communication, as it accurately models the coexistence of LOS and NLOS signal components present in the satellite signals [41]. According to Rician fading model, (1) can be rewritten as

$$\mathbf{H}_{m,k}^{\text{sat}} = \bar{\mathbf{H}}_{m,k} + \tilde{\mathbf{H}}_{m,k}. \quad (6)$$

In the case of LOS communication, the deterministic LOS component $\bar{\mathbf{H}}_{m,k} = \sqrt{\kappa_k\beta_k/(\kappa_k+1)}\mathbf{g}_{m,k,1}\mathbf{h}_{m,k}^{\text{H}}$ has much larger power than the scattering component $\tilde{\mathbf{H}}_{m,k} = \sqrt{\beta_k/(\kappa_k+1)}\tilde{\mathbf{g}}_{m,k}\mathbf{h}_{m,k}^{\text{H}}$. To characterize the dominance of LOS component over the NLOS ones, typically the Rician factor is set such as $10\log(\kappa_k) \approx 10$ dB [8] [9]. As for the scattering component, $\tilde{\mathbf{g}}_{m,k} \sim \mathcal{CN}(0, \boldsymbol{\Sigma}_{m,k})$ with $\text{tr}(\boldsymbol{\Sigma}_{m,k}) = 1$. We focus on the LOS case and devise beamforming algorithms that are based on $\bar{\mathbf{H}}_{m,k}$.

The LEO satellites are operated on fixed orbits. Satellite orbits and visibility at a given location on earth can be predicted accurately using standard software. Combined with

the real-time observations obtained from the Telemetry, Tracking and Control subsystem [42] which constantly monitors the states of satellites, the trajectories of satellites can be assumed to be available at the transmitter side so that accurate information on $\bar{\mathbf{H}}_{m,k}$ can be predicted and gathered at one satellite platform, which then employs its on-board processor to solve the beamforming problem and disseminate $\mathbf{d}_k, \mathbf{v}_k$ to the corresponding transmitters and receivers.

We assume two types of heterogeneous receivers, with $\sigma_{i,1} > \sigma_{i,2}$. Each weaker ground terminal $t_{i,1}$ is paired with a stronger one $t_{i,2}$ and there is a total of I pairs. A detailed pairing method is out of the scope of this paper, but in the case of satellite to ground LOS communication, a convenient way of pairing is simply based on the distance between $t_{i,1}$ and $t_{i,2}$. Terminals $t_{i,1}$ and $t_{i,2}$ are allocated with transit beamformer $\mathbf{d}_{i,1}$, $\mathbf{d}_{i,2}$ and receiving beamformer $\mathbf{v}_{i,1}, \mathbf{v}_{i,2}$ to achieve QoSs of $r_{i,1}, r_{i,2}$ b/s/Hz respectively. Likewise, $\mathbf{H}_{i,1}$, $\mathbf{H}_{i,2}$ represent the channels for the weaker and the stronger terminals in group i. We assume that $Mn_r \geq N_{\text{tot}} = 2I$.

The signal-to-noise-ratio (SINR) $\gamma_{i,j}$ relates to $r_{i,j}$ such that

$$\log(1 + \gamma_{i,j}) = r_{i,j}. \tag{7}$$

We define $\mathcal{P}(\boldsymbol{\gamma}|\mathbf{H}_{i,1}, \mathbf{H}_{i,2}, i = 1, \cdots, I)$ as the function which is parameterized by the channel information. $\mathcal{P}$ maps the QoSs into the minimum transmission power required at the satellite transmitters. To ascertain the value $\mathcal{P}$ for a particular $\boldsymbol{\gamma}$ amounts to solving the QoS constrained minimum power beamforming optimization, which as will be formulated in Section II-C, is the major optimization problem focused by this paper. This type of optimization by itself is meaningful in that the satellites are power limited and the services are usually of a heterogeneous nature. We introduce a motivational model below to further suggest that $\mathcal{P}$ also provides essential knowledge for cross-layer optimization in the integrated space-terrestrial network.

Although in practice there could be multiple links between $t_{i,1}$ and $t_{i,2}$, without loss of generality (w.l.o.g), we use only one link l_i to model the constraint of the terrestrial networks, through which the stronger terminal and the weaker terminal are connected. An upper transmission rate limit c_i is ascribed to l_i. Suppose the LEO satellite network is requested to deliver a rate of r_i^{LEO} towards $t_{i,1}$. The total flow can be split such that the satellites respectively transmit at a speed of $r_{i,1} = r_i^{LEO} - r_{i,2}$ and $r_{i,2}$ towards $t_{i,1}$ and $t_{i,2}$, with the latter sub-flow being relayed through l_i from $t_{i,2}$ to $t_{i,1}$. Denote the rate for terrestrial services that go through l_i as r_i^{TER}, therefore $r_{i,2} + r_i^{TER} \leq c_i$. In contrast to r_i^{LEO}, which is specified by the QoS request from the satellite user, we assume that the terrestrial services generate elastic traffic, i.e. r_i^{TER} is optimized to maximize the corresponding network utility. One common metric widely used in the Network Utility Maximization (NUM) literature [35] for quantifying the network utility is the proportional fairness metric,

$$U_i\left(r_i^{TER}\right) = \log(r_i^{TER}), i = 1, \cdots, I. \tag{8}$$

Intuitively, the larger of the offloading data rate $r_{i,2}$ at the expense of lowering U_i is, the less transmission power $\mathcal{P}$ is taken. The following global optimization problem is proposed to characterize such a trade-off between maximizing U_i and minimizing $\mathcal{P}$,

$$\max_{\boldsymbol{\gamma} \geq 0, r_i^{TER}} \sum_{i=1}^{I} U_i\left(r_i^{TER}\right) - w\mathcal{P}(\boldsymbol{\gamma}) \tag{9}$$

$$\text{s.t. } r_{i,2} \leq r_i^{LEO} \tag{10}$$

$$r_{i,2} + r_i^{TER} \leq c_i, \tag{11}$$

$$\log(1 + \gamma_{i,2}) = r_{i,2},\ i = 1, \cdots, I,$$

where w is the weighting factor, set by the operator to control the relative importance of the transmission power with respect to (w.r.t) U_i. To find the solution to (9), gradient based searching algorithms are the state of the art methods. It has been well documented in the NUM literature [35] that the gradient of the network utility can be obtained efficiently in a decentralized manner through primal decomposition. Therefore, to solve the cross-layer optimization in (9), it is left only to compute the gradient for $\mathcal{P}$ w.r.t $\boldsymbol{\gamma}$, which as proved later in Subsection III-A, is linked to solving the QoS constrained beamforming problem, which will be introduced in the next section.

C. Minimum Power Beamforming Optimization with QoS Constraints and NOMA

The mapping from SINRs to transmission power, i.e. $\mathcal{P}(\boldsymbol{\gamma})$ can be written explicitly as the minimum power beamforming optimization. Fixing the receiving beamformer $\mathbf{v}_{i,j} = \bar{\mathbf{v}}_{i,j}, j = 1, 2$, define the effective channel for each receiver in pair i as $\tilde{\mathbf{h}}_{i,j} = \bar{\mathbf{v}}_{i,j}^{\mathrm{H}} \mathbf{H}_{i,j} \bar{\mathbf{W}}, j = 1, 2$. The QoS constrained beamforming optimization can be formulated as

$$\min_{\mathbf{D}} \sum_{i=1}^{I} \|\mathbf{d}_{i,1}\|^2 + \|\mathbf{d}_{i,2}\|^2 \tag{12}$$

$$\text{s.t. } \text{SINR}_i^{1-1} = \frac{\|\widetilde{\mathbf{h}}_{i,1}^{\mathrm{H}} \mathbf{d}_{i,1}\|^2}{\zeta_{i,1} + \|\widetilde{\mathbf{h}}_{i,1}^{\mathrm{H}} \mathbf{d}_{i,2}\|^2 + \sigma_{i,1}^2} \geq \gamma_{i,1}, \tag{13}$$

$$\text{SINR}_i^{2-1} = \frac{\|\widetilde{\mathbf{h}}_{i,2}^{\mathrm{H}} \mathbf{d}_{i,1}\|^2}{\zeta_{i,2} + \|\widetilde{\mathbf{h}}_{i,2}^{\mathrm{H}} \mathbf{d}_{i,2}\|^2 + \sigma_{i,2}^2} \geq \gamma_{i,1}, \tag{14}$$

$$\text{SINR}_i^{2-2} = \frac{\|\widetilde{\mathbf{h}}_{i,2}^{\mathrm{H}} \mathbf{d}_{i,2}\|^2}{\zeta_{i,2} + \sigma_{i,2}^2} \geq \gamma_{i,2}, \text{for } i = 1 \cdots I. \tag{15}$$

The values SINR_i^{1-1} and SINR_i^{2-1} are respectively the SINRs obtained at the weaker and the stronger users in group i for decoding the weaker user's message, whereas SINR_i^{2-2} is the SINR achieved at the stronger user when decoding the stronger user's message. Constraint (14) is set to ensure that terminal $t_{i,2}$ can decode and subtract out the weaker user's message using SIC. Scalars $\zeta_{i,k}, k = 1, 2$ specify the inter-pair interference. In reality, only signals transmitted to nearby pairs of receivers would form non-negligible inter-pair interference. This motivates us to use an approximation of $\zeta_{i,k}$, such that

$$\zeta_{i,1} = \sum_{j \in \mathcal{N}(i)} \|\widetilde{\mathbf{h}}_{i,1}^{\mathrm{H}} \mathbf{d}_{j,1}\|^2 + \sum_{j \in \mathcal{N}^s(i)} \|\widetilde{\mathbf{h}}_{i,1}^{\mathrm{H}} \mathbf{d}_{j,2}\|^2, \tag{16}$$

$$\zeta_{i,2} = \sum_{j \in \mathcal{M}(i)} \|\widetilde{\mathbf{h}}_{i,2}^{\mathrm{H}} \mathbf{d}_{j,1}\|^2 + \sum_{j \in \mathcal{M}^s(i)} \|\widetilde{\mathbf{h}}_{i,2}^{\mathrm{H}} \mathbf{d}_{j,2}\|^2. \tag{17}$$

where the threshold parameter η is used to control the accuracy of the approximation, sets $\mathcal{N}(i) = \{j \mid \|\widetilde{\mathbf{h}}_{i,1}^{\mathrm{H}}\mathbf{d}_{j,1}\|^2/(\|\widetilde{\mathbf{h}}_{i,1}\|\|\mathbf{d}_{j,1}\|) > \eta,\ j \neq i\}$, and similarly $\mathcal{N}^s(i) = \{j \mid \|\widetilde{\mathbf{h}}_{i,1}^{\mathrm{H}}\mathbf{d}_{j,2}\|^2/(\|\widetilde{\mathbf{h}}_{i,1}\|\|\mathbf{d}_{j,2}\|) > \eta,\ j \neq i\}$ are defined as the indexes of users that form non-negligible interference to the weaker user i. Similar definitions are applied to $\mathcal{M}$ and $\mathcal{M}^s$ to specify respectively the clusters of the weaker and the stronger users which generate interfering signals against stronger users.

D. Joint Uplink and Downlink MIMO optimization

Fix the digital beamformers $\mathbf{d}_{i,j} = \bar{\mathbf{d}}_{i,j}$ for $i = 1, \cdots, I, j = 1, 2$. The effective channel for the reception of the signal intended for $t_{k,l}$ at $t_{i,j}$ can be written as

$$\hat{\mathbf{h}}_{k,l}^{i,j} = \mathbf{H}_{i,j}\bar{\mathbf{W}}\bar{\mathbf{d}}_{k,l}. \tag{18}$$

In cases where it is clear which receiver we are referring to, the superscript of $\hat{\mathbf{h}}_{k,l}^{i,j}$ will be dropped. At the weaker terminal $t_{i,1}$, choose the receiving beamformer from the discrete codebook $\mathcal{V}$, such as

$$\max_{\mathbf{v}\in\mathcal{V}} \quad \mathrm{SINR}_i^{1-1} \tag{19}$$

$$= \frac{\|\mathbf{v}^{\mathrm{H}}\hat{\mathbf{h}}_{i,1}\|^2}{\sum_{k\neq i}\|\mathbf{v}^{\mathrm{H}}\hat{\mathbf{h}}_{k,1}\|^2 + \sum_{k=1}^{I}\|\mathbf{v}^{\mathrm{H}}\hat{\mathbf{h}}_{k,2}\|^2}. \tag{20}$$

The design of $\mathcal{V}$ is discussed in more detail in Section III-D. At the stronger terminal $t_{i,2}$, $\mathbf{v}$ is chosen such that

$$\max_{\mathbf{v}\in\mathcal{V}} \quad \mathrm{SINR}_i^{2-2} \tag{21}$$

$$= \frac{\|\mathbf{v}^{\mathrm{H}}\hat{\mathbf{h}}_{i,2}\|^2}{\sum_{k=1}^{I}\|\mathbf{v}^{\mathrm{H}}\hat{\mathbf{h}}_{k,1}\|^2 + \sum_{k\neq i}\|\mathbf{v}^{\mathrm{H}}\hat{\mathbf{h}}_{k,2}\|^2} \tag{22}$$

$$\text{s.t.} \quad \frac{\|\mathbf{v}^{\mathrm{H}}\hat{\mathbf{h}}_{i,1}\|^2}{\sum_{k\neq i}\|\mathbf{v}^{\mathrm{H}}\hat{\mathbf{h}}_{k,1}\|^2 + \sum_{k=1}^{I}\|\mathbf{v}^{\mathrm{H}}\hat{\mathbf{h}}_{k,2}\|^2} \geq \gamma_{i,1}. \tag{23}$$

While satisfying the SIC constraint, the optimization from (21) will produce the receiving beamformer at $t_{i,2}$ that maximizes SINR_i^{2-2}. Through the iterations of solving the transmit and the receive beamforming optimization problems of (12), (19) and (21), the transmission power is minimized while still meeting the QoS constraints in (13)-(15).

III. Optimization Problem Analysis and Decentralized Implementation

In this section, we first analyze the optimality for (12) as well as its role in solving the cross-layer optimization (9). Then we concentrate on the design of the decentralized algorithm for solving (12). It is worth noting that the derivation of the distributed algorithm proposed in this paper does not rely on specific assumptions on channel models or the existence of LOS component. Finally, a novel complexity reduction method based on DNNs is proposed.

A. Optimality of the QoS Constrained Minimum Power beamforming with NOMA

Introduce the dual variables $\mu_{i,1}, \mu_{i,2}, \mu_{i,3}$ for constraints (13),(14) and (15). The corresponding Lagrangian function can be written as

$$\mathcal{L}(\mathbf{d}, \mu) = \sum_{i=1}^{I}\left\{\mathbf{d}_{i,1}^{\mathrm{H}}\mathbf{P}_i\mathbf{d}_{i,1} + \mu_{i,1}\sigma_{i,1}^2 + \mu_{i,2}\sigma_{i,2}^2\right\} + \sum_{i=1}^{I}\left\{\mathbf{d}_{i,2}^{\mathrm{H}}\mathbf{Q}_i\mathbf{d}_{i,2} + \mu_{i,3}\sigma_{i,2}^2\right\}, \tag{24}$$

where $\mathbf{P}_i$ and $\mathbf{Q}_i$ are N by N matrices with $N = MN_s$. To write these two matrices explicitly, we further introduce the definitions $\mathcal{N}_c(i) = \{j | i \in \mathcal{N}(j), j = 1, \cdots, I\}$, $\mathcal{N}_c^s(i) = \{j | i \in \mathcal{N}^s(j), j = 1, \cdots, I\}$ for $\mathcal{N}_c(i), \mathcal{N}_c^s(i)$ and likewise for $\mathcal{M}_c(i)$, $\mathcal{M}_c^s(i)$. Denote the cardinality of set $\hat{\mathcal{N}}_c(i) = \mathcal{N}_c(i) \cup \mathcal{N}_c^s(i)$ and $\hat{\mathcal{M}}_c(i) = \mathcal{M}_c(i) \cup \mathcal{M}_c^s(i)$ respectively such as $n_{i,1}$ and $n_{i,2}$. Finally we obtain

$$\mathbf{P}_i = \sum_{j\in\mathcal{N}_c(i)}\mu_{j,1}\widetilde{\mathbf{h}}_{j,1}\widetilde{\mathbf{h}}_{j,1}^{\mathrm{H}} + \sum_{j\in\mathcal{M}_c(i)}(\mu_{j,2}+\mu_{j,3})\widetilde{\mathbf{h}}_{j,2}\widetilde{\mathbf{h}}_{j,2}^{\mathrm{H}} - \frac{\mu_{i,1}}{\gamma_{i,1}}\widetilde{\mathbf{h}}_{i,1}\widetilde{\mathbf{h}}_{i,1}^{\mathrm{H}} - \frac{\mu_{i,2}}{\gamma_{i,1}}\widetilde{\mathbf{h}}_{i,2}\widetilde{\mathbf{h}}_{i,2}^{\mathrm{H}} + \mathbf{I}, \tag{25}$$

$$\mathbf{Q}_i = \sum_{j\in\mathcal{N}_c^s(i)}\mu_{j,1}\widetilde{\mathbf{h}}_{j,1}\widetilde{\mathbf{h}}_{j,1}^{\mathrm{H}} + \sum_{j\in\mathcal{M}_c^s(i)}(\mu_{j,2}+\mu_{j,3})\widetilde{\mathbf{h}}_{j,2}\widetilde{\mathbf{h}}_{j,2}^{\mathrm{H}} - \frac{\mu_{i,3}}{\gamma_{i,2}}\widetilde{\mathbf{h}}_{i,2}\widetilde{\mathbf{h}}_{i,2}^{\mathrm{H}} + \mu_{i,1}\widetilde{\mathbf{h}}_{i,1}\widetilde{\mathbf{h}}_{i,1}^{\mathrm{H}} + \mu_{i,2}\widetilde{\mathbf{h}}_{i,2}\widetilde{\mathbf{h}}_{i,2}^{\mathrm{H}} + \mathbf{I} \tag{26}$$

By minimizing (24) w.r.t $\mathbf{d}$ and then maximize over the dual variables , the dual optimization of (12) is

$$\max_{\boldsymbol{\mu}}\ q(\boldsymbol{\mu}) = \sum_{i=1}^{I}\mu_{i,1}\sigma_{i,1}^2 + (\mu_{i,2}+\mu_{i,3})\sigma_{i,2}^2, \tag{27}$$

$$\mathbf{P}_i, \mathbf{Q}_i \in \mathbf{S}_+^N \text{ for } i = 1, \cdots, I, \tag{28}$$

$$\boldsymbol{\mu} \geq 0. \tag{29}$$

Notice that (27) forms a semidefinite programme, also known as a linear matrix inequalities (LMI) program. Various types of interior points algorithms are well known to solve such problems efficiently [26]. However, with a large amount of users requiring to be served in real time, (27) with high-dimensional $\mathbf{P}_i$, $\mathbf{Q}_i$ and a large number of user pairs I, needs to be solved in real time, which is very challenging.

Proposition 1: Problems (12) and (27) achieve the same optimal value, i.e. strong duality holds for (12). The optimal duals for (27), $\mu_{i,1}^*, \mu_{i,2}^*, \mu_{i,3}^*, i = 1, \cdots, I$, are identical with those for the optimization problem (71) (introduced in Appendix A).

Proof: See Appendix A. ∎

Based on Proposition 1, the Karush–Kuhn–Tucker (KKT) point of (12) is the optimum solution, although (12) is non-convex. We can first solve its dual (27), which is concave. Based on the optimal duals $\boldsymbol{\mu}^*$, the optimal primal variables $\mathbf{d}^*$ can be traced back according to the optimality conditions, such as illustrated in Appendix B.

With Proposition 2, we show that the gradient information $\partial\mathcal{P}/\partial\boldsymbol{\gamma}$ is related to the optimal dual variables for (27).

Proposition 2: Given a fixed receiving beamformer $\bar{\mathbf{v}}_{i,j}$ for $i = 1, \cdots, I, j = 1, 2$, provided $\widetilde{\mathbf{h}}_{i,1}, \widetilde{\mathbf{h}}_{i,2}, i = 1, \cdots, I$ are linearly independent from each other, the gradient of $\mathcal{P}(\boldsymbol{\gamma})$ is computed as

$$\partial\mathcal{P}/\partial\gamma_{i,1} = -\mu_{i,1} - \mu_{i,2}, \partial\mathcal{P}/\partial\gamma_{i,2} = -\mu_{i,3}, i = 1, \cdots, I.$$

Proof: See Appendix C. ∎

In the gradient based searching algorithm to solve (9), in order to obtain the gradient information w.r.t $\boldsymbol{\gamma}$, (27) needs to be solved at each iteration of the sub-gradient algorithm. Therefore, it is important to have a low-complexity solution for (27) so that real-time solutions to the cross-layer optimization in (9) can be obtained.

B. Decentralization through double dual relaxation

Inspired by [27], we decentralize the dual problem (27) through constraint relaxation and dual decomposition. For each $\mathbf{P}_i$ and $\mathbf{Q}_i$, introduce their local versions $\mathbf{P}_i^{lo}$, $\mathbf{Q}_i^{lo}$ that are matrices of the following optimization variables

$$\boldsymbol{\mu}_i^l = \left[\mu_{i,1}, \mu_{i,2}, \mu_{i,3}, \boldsymbol{\mu}_{i,1}^l, \boldsymbol{\mu}_{i,2}^l\right], \tag{30}$$

where $\boldsymbol{\mu}_{i,1}^l$ represents the local copies for all the related $\mu_{j,1}, j \in \hat{\mathcal{N}}_c(i)$, and $\boldsymbol{\mu}_{i,2}^l$ represents $\mu_{j,2}+\mu_{j,3}$ for $j \in \hat{\mathcal{M}}_c(i)$. The number of the elements in $\boldsymbol{\mu}_i^l$ is therefore $n_i = 3+n_{i,1}+n_{i,2}$. The relaxed dual problem with matrices $\mathbf{P}_i^{lo}$, $\mathbf{Q}_i^{lo}$ can be written explicitly as

$$\max_{\boldsymbol{\mu}_i^l} \sum_{i=1}^{I} \mu_{i,1}\sigma_{i,1}^2 + (\mu_{i,2}+\mu_{i,3})\sigma_{i,2}^2 \tag{31}$$

$$\text{s.t.} \quad \mathbf{P}_i^{lo}, \mathbf{Q}_i^{lo} \in \mathbf{S}_+^N, \text{for } i = 1, \cdots, I, \tag{32}$$

$$\boldsymbol{\mu}_i^l \geq 0. \tag{33}$$

The local copies, $\boldsymbol{\mu}_{i,1}^l$, $\boldsymbol{\mu}_{i,2}^l$ are made to be connected globally following the equations below,

$$\mu_{i,k,1}^l = \mu_{k,1}, k \in \hat{\mathcal{N}}_c(i), \tag{34}$$

$$\mu_{i,k,2}^l = \mu_{k,2} + \mu_{k,3}, k \in \hat{\mathcal{M}}_c(i), \tag{35}$$

where $\mu_{i,k,1}^l, \mu_{i,k,2}^l$ are entries of $\boldsymbol{\mu}_{i,1}^l$ and $\boldsymbol{\mu}_{i,2}^l$. The original dual problem (27) is now decomposed into I separate LMI programs with global linear constraints, i.e. (34), (35), written in vector form such as $\boldsymbol{\mu}_{i,1}^l = \boldsymbol{\mu}_{i,1}^{gl}, \boldsymbol{\mu}_{i,2}^l = \boldsymbol{\mu}_{i,2}^{gl}$, or

$$\sum_i^I \mathbf{A}_i \boldsymbol{\mu}_i^l = \mathbf{b}, \tag{36}$$

where $\mathbf{b}$ is a zero column vector, $\mathbf{A}_i \in \mathbb{R}^{n_0 \times n_i}$ with $n_0 = \sum_{i=1}^{I}(n_{i,1}+n_{i,2})$.

It is now possible to apply the dual decomposition technique to the global constraints (34) and (35), i.e. ascribing dual variables to these constraints and forming the corresponding dual problem to (31). Notice that the optimality of the original problem would be preserved after the dual decomposition since (31) is convex and the duality gap is zero between the original convex problem and its dual problem [26].

Numerical experiments indicate that two of the popular distributed algorithms, subgradient descent [28] and Alternating Direction Method of Multipliers (ADMM) [29] actually fail to converge. We propose a distributed version of the augmented Lagrangian method that succeeds in solving problem (31). The augmented Lagrangian function for (31) is

$$\Lambda_\rho(\boldsymbol{\mu}, \boldsymbol{\lambda}) = \sum_{i=1}^{I}\Bigg(F_i(\boldsymbol{\mu}_i^l) + \sum_{s=1}^{2}\Big(\boldsymbol{\lambda}_{i,s}^{\mathrm{T}}(\boldsymbol{\mu}_{i,s}^l - \boldsymbol{\mu}_{i,s}^{gl}) - \frac{\rho}{2}\|\boldsymbol{\mu}_{i,s}^l - \boldsymbol{\mu}_{i,s}^{gl}\|^2\Big)\Bigg), \tag{37}$$

where $\rho > 0$, $\boldsymbol{\lambda}_{i,s}, s = 1, 2$, are the duals for the corresponding linear constraints, i.e. satisfying the complementary condition at the optimal point as

$$\lambda_{i,k,1}(\mu_{i,k,1}^l - \mu_{k,1}) = 0, k \in \hat{\mathcal{N}}_c(i), \tag{38}$$

$$\lambda_{i,k,2}(\mu_{i,k,2}^l - \mu_{k,2} - \mu_{k,3}) = 0, k \in \hat{\mathcal{M}}_c(i). \tag{39}$$

$F_i(\boldsymbol{\mu}_i^l)$ is the indicator function

$$F_i(\boldsymbol{\mu}_i^l) = \begin{cases} \mu_{i,1}\sigma_{i,1}^2 + (\mu_{i,2}+\mu_{i,3})\sigma_{i,2}^2, & \mathbf{P}_i^{lo}, \mathbf{Q}_i^{lo} \in \mathbf{S}_+^N, \\ -\infty, & \text{otherwise.} \end{cases} \tag{40}$$

The distributed algorithm is implemented such as described in Algorithm 1. The total process is divided into computations at I nodes in parallel. One node corresponds to one pair of users. The objective function of (41) is a quadratic function of $\boldsymbol{\mu}_i^l$ with

$$\Lambda_i(\boldsymbol{\mu}_i^l) = \mu_{i,1}\sigma_{i,1}^2 + (\mu_{i,2}+\mu_{i,3})\sigma_{i,2}^2 + \sum_{s=1}^{2}\Big(\boldsymbol{\lambda}_{i,s}^{\mathrm{T}}(\boldsymbol{\mu}_{i,s}^l - \boldsymbol{\mu}_{i,s}^{gl}) - \frac{\rho}{2}\|\boldsymbol{\mu}_{i,s}^l - \boldsymbol{\mu}_{i,s}^{gl}\|^2\Big). \tag{46}$$

Algorithm 1 Distributed Algorithm for NOMA beamforming

1: Initialization: Set initial values for $\boldsymbol{\lambda}_{i,k} = \boldsymbol{\lambda}_{i,k}^{t=0}, k = 1, 2$ and for $\boldsymbol{\mu}_i^l = \boldsymbol{\mu}_i^{l,t=0}, i = 1, \cdots, I, t = 1$.

2: At each node i, for $i = 1, \cdots, I$, compute the solution $\hat{\boldsymbol{\mu}}_i^{l,t-1}$ for the following problem

$$\max_{\boldsymbol{\mu}_i^l} \quad \Lambda_i(\boldsymbol{\mu}_i^l) + \sum_{n\in\mathcal{X}_1(i)}\Big(\lambda_{n,i,1}(\mu_{n,i,1}^l - \mu_{i,1}) + \frac{\rho}{2}(\mu_{n,i,1}^l - \mu_{i,1})^2\Big) + \sum_{n\in\mathcal{X}_2(i)}\Big(\lambda_{n,i,2}(\mu_{n,i,2}^l - \mu_{i,2} - \mu_{i,3}) + \frac{\rho}{2}(\mu_{n,i,2}^l - \mu_{i,2} - \mu_{i,3})^2\Big) \tag{41}$$

$$\text{s.t.} \quad \mathbf{P}_i^{lo}, \mathbf{Q}_i^{lo} \in \mathbf{S}_+^N \tag{42}$$

$$\boldsymbol{\mu}_i^l \geq 0. \tag{43}$$

with $\mathcal{X}_1(i) = \mathcal{N}(i) \cup \mathcal{N}^s(i)$, $\mathcal{X}_2(i) = \mathcal{M}(i) \cup \mathcal{M}^s(i)$.

3: At each node i for $i = 1, \cdots, I$, update $\boldsymbol{\mu}_i^l$ according to

$$\boldsymbol{\mu}_i^{l,t} = \boldsymbol{\mu}_i^{l,t-1} + \tau(\hat{\boldsymbol{\mu}}_i^{l,t-1} - \boldsymbol{\mu}_i^{l,t-1}). \tag{44}$$

4: At each node i, for $i = 1, \cdots, I$, update $\boldsymbol{\lambda}$ according to

$$\boldsymbol{\lambda}_{i,k}^t = \boldsymbol{\lambda}_{i,k}^{t-1} + \rho\tau(\boldsymbol{\mu}_{i,k}^{l,t} - \boldsymbol{\mu}_{i,k}^{gl,t}), \text{for } k = 1, 2. \tag{45}$$

Increase t by 1 and return to Step 2 until convergence condition is met.

According to [30], the convergence is guaranteed as long as $\tau \in (0, \frac{1}{2})$ in (44) and (45). More theoretical and numerical results on the convergence will be provided in the next section as well as in the simulation results.

One simplification can be made about Algorithm 1. Due to the decentralized implementation, the channel vectors contained in $\mathbf{P}_i^{lo}$, $\mathbf{Q}_i^{lo}$, which dictate the dimensions of the matrix inequality in the sub problem (41), can be projected onto another sub-space through QR decomposition,

$$\mathbf{H}_i^l = \left[\tilde{\mathbf{h}}_{i,1}, \tilde{\mathbf{h}}_{i,2}, \mathbf{H}_{i,1}^l, \mathbf{H}_{i,2}^l\right] = \mathbf{Q}_i \mathbf{R}_i, \tag{47}$$

where the j^{th} column of $\mathbf{H}_{i,1}^l$ contains $\tilde{\mathbf{h}}_{j,1}$, $j = \hat{\mathcal{N}}_c(i)|_j$, the j^{th} column of $\mathbf{H}_{i,2}^l$ contains $\tilde{\mathbf{h}}_{j,2}$, $j = \hat{\mathcal{M}}_c(i)|_j$. $\mathbf{R}_i$ is a square matrix. Its a total of $2+n_{i,1}+n_{i,2}$ columns can be substituted in (32). This results in a dimension change in the inequality constraint from $2I$ to $2+n_{i,1}+n_{i,2}$. For multi-beam satellite networks, a large number of users are served while the number of adjacent interfering users is a lot smaller, indicating that I is typically much larger than $n_{i,1}+n_{i,2}$.

C. Complexity Reduction through Approximation Methods for Convex Optimizations

In Algorithm 1, the most computational burden lies in solving the subproblem (41), denoted as $\mathcal{P}_i$, while the complexity requested in other operations such as in (44), (45), is trivial. Problem $\mathcal{P}_i$ is strongly convex. The barrier method, which is a typical type of interior point algorithm, can be used to deal with the linear matrix inequality constraints in $\mathcal{P}_i$ [26]. A detailed implementation is given in Algorithm 2.

Algorithm 2 The barrier method for the local LMI constrained problem

Initialization: Given $\epsilon > 0$, $\alpha > 1$, $\omega = \omega^{t=0} > 0$ and a strictly feasible $\boldsymbol{\mu}_i^l = \boldsymbol{\mu}_i^{l,t=0}$, i.e. $\mathbf{P}_i^{lo}(\boldsymbol{\mu}_i^{l,t=0}), \mathbf{Q}_i^{lo}(\boldsymbol{\mu}_i^{l,t=0}) \in \mathbf{S}_+^N$.
Repeat:

1: $t = t + 1$.
2: Use any descent method to solve the following unconstrained problem with $\boldsymbol{\mu}_i^{l,t-1}$ as the starting point

$$\max_{\boldsymbol{\mu}_i^l} \omega^{t-1} q_i(\boldsymbol{\mu}_i^l) + \phi_i(\boldsymbol{\mu}_i^l), \tag{48}$$

where $q_i(\boldsymbol{\mu}_i^l)$ is the objective function in (41), ϕ_i is the barrier function

$$\phi_i = \log\left(\det \mathbf{P}_i^{lo} \det \mathbf{Q}_i^{lo} \prod_{k=1}^{n_i} \boldsymbol{\mu}_i^l|_k\right). \tag{49}$$

3: Update: $\boldsymbol{\mu}_i^{l,t} = \boldsymbol{\mu}_i^*$.
4: Stopping criterion: Loop ends if $1/\omega^{t-1} < \epsilon$.
5: Increase ω: $\omega^t = \omega^{t-1}\alpha$.

Algorithm 2 consists of two loops: the outer loop where ω is incrementally increased and the inner loop where an iterative searching algorithm is applied to solve (48). Projecting the channel vectors in $\mathbf{P}_i^{lo}$ and $\mathbf{Q}_i^{lo}$ onto the column space of $\mathbf{R}_i$ from (47), each iteration of the descent method in (48) can be greatly simplified, since now $\mathbf{P}_i^{lo}, \mathbf{Q}_i^{lo} \in \mathbf{S}_+^{2+n_{i,1}+n_{i,2}}$. Newton's method is typically used as the descent method for (48) and the cost of one iteration is order $(n_{i,1}+n_{i,2})^4$. The original dual problem (27) (before implementation in a distributed fashion) is also LMI program. When solved by the barrier method similar to Algorithm 2, the cost of each iteration is order I^4, which is much higher compared to $(n_{i,1}+n_{i,2})^4$ in the scenarios of multi-beam satellite communications.

To further reduce the complexity, we propose to use some approximation methods that, while produce only the approximations of the solutions generated by Algorithm 2, have lower complexity. Before delving into the actual approximation technique, the impact of approximation error, i.e. $(\hat{\boldsymbol{\mu}}_{i,\text{approx}}^l - \hat{\boldsymbol{\mu}}_i^l)$, on the convergence property of Algorithm 1 needs to be understood. First introduce $\mathbf{T}_i = \text{diag}(\tau, \cdots, \tau) \in \mathbb{R}^{n_i \times n_i}$ and $\mathbf{T} = \text{diag}(\tau, \cdots, \tau) \in \mathbb{R}^{n_0 \times n_0}$. The residual constraint violation at each iteration in Algorithm 1 is computed such as

$$\mathbf{r}(\boldsymbol{\mu}^{l,t}) = \sum_i^I (\mathbf{A}_i \boldsymbol{\mu}_i^{l,t} - \mathbf{b}). \tag{50}$$

Denote the corresponding Lyapunov function as

$$\phi(\boldsymbol{\mu}^{l,t}, \boldsymbol{\lambda}^t) = \sum_{i=1}^I \rho \|\boldsymbol{\mu}_i^{l,t} - \boldsymbol{\mu}_i^{l,*}\|_{\mathbf{T}_i^{-1}}^2 + \frac{1}{\rho}\|\bar{\boldsymbol{\lambda}}^t - \boldsymbol{\lambda}^*\|_{\mathbf{T}^{-1}}^2, \tag{51}$$

$$\text{with } \bar{\boldsymbol{\lambda}}^t = \boldsymbol{\lambda}^t + \rho(\mathbf{I} - \mathbf{T})\mathbf{r}(\boldsymbol{\mu}^{l,t}), \tag{52}$$

where the matrix norm is computed according to $\|\mathbf{x}\|_{\mathbf{M}} = \sqrt{\mathbf{x}^{\mathrm{H}}\mathbf{M}\mathbf{x}}$, $\boldsymbol{\mu}_i^{l,*}$ and $\boldsymbol{\lambda}^*$ are the optimal points for $\boldsymbol{\mu}_i^{l,t}$ and $\boldsymbol{\lambda}^t$ respectively. We prove in Theorem 1 that with certain restrictions on the approximation error, (51) reduces to zero as the number of iterations increases and $\boldsymbol{\mu}_i^{l,t}$ converges to the optimum. To use a simpler notation, we drop the superscript l in the local optimization variable $\boldsymbol{\mu}_i^{l,t}$ in the rest part of this section. Denote $[\mathbf{A}_i]_j$ as the j^{th} row of $\mathbf{A}_i$. Define d_j as the number of $i = 1, \cdots, I$ such that $[\mathbf{A}_i]_j \neq \mathbf{0}$. d_j is known as the degree of the linear constraints. In the case of our problem (36), $d_j = 2$ for all j.

Assumption 1: Denote $\boldsymbol{\mu}_{i,n}^t$ and $\hat{\boldsymbol{\mu}}_{i,n}^t$ as the noisy versions (with approximation error) of $\boldsymbol{\mu}_i^t$ and $\hat{\boldsymbol{\mu}}_i^t$ respectively. The following two equations connect these variables such as

$$\boldsymbol{\mu}_{i,n}^t = \boldsymbol{\mu}_i^t + e_{i,1}^t(\hat{\boldsymbol{\mu}}_i^{t-1} - \boldsymbol{\mu}_i^{t-1}), \tag{53}$$

$$\boldsymbol{\mu}_{i,n}^t = \boldsymbol{\mu}_i^t + e_{i,2}^t \hat{\boldsymbol{\mu}}_i^{t-1}, \tag{54}$$

where the magnitudes of $e_{i,1}^t, e_{i,2}^t$ are bounded above such as

$$\forall t, i,\ |e_{i,1}^t| \leq \epsilon_{i,1}, |e_{i,2}^t| \leq \epsilon_2. \tag{55}$$

Theorem 1: Under Assumption 1 and provided that $c_1 = \rho(1 - \tau - \epsilon_{i,1}^2/\tau), c_2 = \rho(\tau - 2\tau^2 - 2c) - \rho^2\epsilon_2^2/\tau$ are strictly positive, where $c > 0$, the primal variables $\boldsymbol{\mu}_i^t$ and the dual $\boldsymbol{\lambda}^t$ produced at each iteration of Algorithm 1, with $\hat{\boldsymbol{\mu}}_i^t$ computed approximately, converge to the primal and dual optimal points $\boldsymbol{\mu}_i^*, \boldsymbol{\lambda}^*$ of problem (31) respectively.

Proof: Based on the magnitude restriction on the approximation error in Assumption 1, we can obtain

$$\|\boldsymbol{\mu}_{i,n}^t - \boldsymbol{\mu}_i^*\|^2_{\mathbf{T}_i^{-1}} = \|\boldsymbol{\mu}_i^t + e_{i,1}^t(\hat{\boldsymbol{\mu}}_i^{t-1} - \boldsymbol{\mu}_i^{t-1}) - \boldsymbol{\mu}_i^*\|^2_{\mathbf{T}_i^{-1}} \tag{56}$$

$$\leq \|\boldsymbol{\mu}_i^t - \boldsymbol{\mu}_i^*\|^2_{\mathbf{T}_i^{-1}} + \epsilon_{i,1}^2\|\hat{\boldsymbol{\mu}}_i^{t-1} - \boldsymbol{\mu}_i^{t-1}\|^2_{\mathbf{T}_i^{-1}},\ i = 1, \cdots, I. \tag{57}$$

Similarly, we have

$$\|\bar{\boldsymbol{\lambda}}_n^t - \boldsymbol{\lambda}^*\|^2_{\mathbf{T}^{-1}} = \|\boldsymbol{\lambda}^{t-1} + \rho\mathbf{r}(\boldsymbol{\mu}^t + e_{i,2}^t\hat{\boldsymbol{\mu}}^{t-1})\|^2_{\mathbf{T}^{-1}} \tag{58}$$

$$\leq \|\bar{\boldsymbol{\lambda}}^t - \boldsymbol{\lambda}^*\|^2_{\mathbf{T}^{-1}} + \rho^2\|\epsilon_2\mathbf{r}(\hat{\boldsymbol{\mu}}^{t-1})\|^2_{\mathbf{T}^{-1}}. \tag{59}$$

According to equation (38) in [30], there exists $\kappa > 0$ such that the exact Lyapunov function values from the successive two iterations, without approximation error, can be written in the inequality below

$$\phi(\boldsymbol{\mu}^t, \boldsymbol{\lambda}^t) \leq \phi(\boldsymbol{\mu}^{t-1}, \boldsymbol{\lambda}^{t-1}) - \rho\sum_i^I \|\hat{\boldsymbol{\mu}}_i^{t-1} - \boldsymbol{\mu}_i^{t-1}\|^2_{\mathbf{I}-\mathbf{T}_i}$$

$$- \rho\|\mathbf{r}(\hat{\boldsymbol{\mu}}^{t-1})\|^2_{\mathbf{T}-\mathbf{D}-2\mathbf{C}} - 2\kappa\|\hat{\boldsymbol{\mu}}^k - \boldsymbol{\mu}^*\|^2, \tag{60}$$

where $\mathbf{D} = \mathrm{diag}(d_1\tau^2, \cdots, d_{n_0}\tau^2)$ and $\mathbf{C} = \mathrm{diag}(c, \cdots, c)$ is any diagonal matrix with strictly positive diagonal elements. Adding (56), (58) to (60), we have

$$\phi(\boldsymbol{\mu}_n^t, \boldsymbol{\lambda}_n^t) \leq \phi(\boldsymbol{\mu}^t, \boldsymbol{\lambda}^t) \tag{61}$$

$$+ \sum_i^I \epsilon_{i,1}^2\|\hat{\boldsymbol{\mu}}_i^{t-1} - \boldsymbol{\mu}_i^{t-1}\|^2_{\mathbf{T}_i^{-1}} + \rho^2\|\epsilon_2\mathbf{r}(\hat{\boldsymbol{\mu}}^{t-1})\|^2_{\mathbf{T}^{-1}}$$

$$\leq \phi(\boldsymbol{\mu}^{t-1}, \boldsymbol{\lambda}^{t-1}) + \sum_i^I \left(\frac{\epsilon_{i,1}^2}{\tau} - \rho(1-\tau)\right)\|\hat{\boldsymbol{\mu}}_i^{t-1} - \boldsymbol{\mu}_i^{t-1}\|^2$$

$$+ \left(\frac{\rho^2\epsilon_2^2}{\tau} - \rho(\tau - 2\tau^2 - 2c)\right)\|\mathbf{r}(\hat{\boldsymbol{\mu}}^{t-1})\|^2 - 2\kappa\|\hat{\boldsymbol{\mu}}^k - \boldsymbol{\mu}^*\|^2. \tag{62}$$

Take the summation of $k = 1, 2, \cdots$ for both sides of the inequality (62)

$$\sum_{t=0}^{\infty}\Big[\sum_i^I c_1\|\hat{\boldsymbol{\mu}}_i^{t-1} - \boldsymbol{\mu}_i^{t-1}\|^2 + c_2\|\mathbf{r}(\hat{\boldsymbol{\mu}}^{t-1})\|^2$$

$$+2\kappa\|\hat{\boldsymbol{\mu}}^t - \boldsymbol{\mu}^*\|^2\Big] \leq \phi(\boldsymbol{\mu}^0, \boldsymbol{\lambda}^0). \tag{63}$$

Since $c_1 > 0, c_2 > 0$ and $\phi(\boldsymbol{\mu}^0, \boldsymbol{\lambda}^0)$ is of finite value, $\hat{\boldsymbol{\mu}}^t$ converges to its optimal point. Furthermore, $\boldsymbol{\lambda}^t$ will also converge to the optimum as ϕ is monotonically decreasing and bounded below. ∎

D. Deep Learning Based Methods for Approximating Convex Optimizations

To approximate the subproblem (41) in Algorithm 1, we employ deep neural networks (DNNs), which are feedforward networks with multiple hidden layers [33], for its well-known extraordinary ability of approximating non-linear mappings in high dimensions.

Problem (41) can be parameterized by considering its objective function and constraints respectively. Note that although the objective function is quadratic w.r.t $\boldsymbol{\mu}_i^l$, the coefficients for the second-order terms are actually fixed. Therefore, an n_i-dimensional vector $\mathbf{p}_i^o$ suffices to parameterize the objective function. As for the constraints, note that $\mathbf{P}_i^{lo}, \mathbf{Q}_i^{lo}$ depend on the QoS thresholds $\gamma_{i,1}, \gamma_{i,2}$ and the effective channels,

$$\tilde{\mathbf{h}}_{i,j}^t = \bar{\mathbf{v}}_{i,j}^{\mathrm{H}}\mathbf{H}_{i,j}^t\bar{\mathbf{W}}^t, j = 1, 2, \tag{64}$$

where t is added to indicate the temporal variability. Since this paper focuses on the LOS cases, $\mathbf{H}_{i,j}^t$ is dominated by the channel geometry and the rain attenuation factor ξs in (2). Assuming that the weaker and the strong user within our group are subject to the same ξs from the satellites, we can parameterize $\mathbf{H}_{i,1}^t\bar{\mathbf{W}}^t, \mathbf{H}_{i,2}^t\bar{\mathbf{W}}^t$ by $\mathbf{p}_i^h = [t, \boldsymbol{\xi}]$, where $\boldsymbol{\xi}$ includes the rain attenuation factors for all effective satellites (remember that $\bar{\mathbf{W}}^t$ is predetermined).

In order for the beam-edge terminal to be served by multiple satellites, beam-splitting can be added to the design of the codebook $\mathcal{V}$ for receiving beamformers. The total antenna elements are split into two parts, $N_u = N_{i,1}^a + N_{i,1}^b$, each generated a beam towards $[\phi_{i,1}^{x,a}, \phi_{i,1}^{y,a}]$ such as

$$\mathbf{v}_a(N_{i,1}^a, \phi_{i,1}^{x,a}, \phi_{i,1}^{y,a}) = \tag{65}$$

$$\big[[1, \ldots, e^{j\pi[(n^x-1)\cos u_{i,1}^a + (n^y-1)\cos v_{i,1}^a]},$$

$$\ldots, e^{j\pi[(N_{i,1}^{x,a}-1)\cos u_{i,1}^a + ((N_{i,1}^{y,a}-1)\cos v_{i,1}^a]}\big]\frac{1}{\sqrt{N_u}},$$

where $\cos u = \sin\phi^x\cos\phi^y$ $\cos v = \sin\phi^x\sin\phi^y$. and the other beam $\mathbf{v}_b(N_{i,1}^b, \phi_{i,1}^{x,b}, \phi_{i,1}^{y,b})$ is expressed in a similar way. The receiving beamformer $\mathbf{v}_{i,1} = [\mathbf{v}_a, \mathbf{v}_b]$ can thus be parameterized by $\mathbf{p}_i^{v,1} = [N_{i,1}^a, \phi_{i,1}^{x,a}, \phi_{i,1}^{y,a}, N_{i,1}^b, \phi_{i,1}^{x,b}, \phi_{i,1}^{y,b})]$. In practice, $\mathbf{v}_a, \mathbf{v}_b$ may respectively point towards two LEO satellites if the ground terminal is on the edge of the beam, or $\mathbf{v}_a, \mathbf{v}_b$ may degenerate into one analogue beam if the terminal is closer to the beam center. To simplify the parameterization and without loss of generality, a fixed uplink beamforming scheme will be assumed. The optimization (41) at node i can thus be modeled as the mapping f_i from $\mathbf{p}_i$ to $\hat{\boldsymbol{\mu}}_i$

$$\hat{\boldsymbol{\mu}}_i \leftarrow f_i\left(\mathbf{p}_i^o, \mathbf{p}_i = [\gamma_{i,1}, \gamma_{i,2}, \mathbf{p}_i^h]\right). \tag{66}$$

Note that $\mathbf{p}_i^o$ varies between iterations of Algorithm 1, while the other ones in $\mathbf{p}_i$ stay the same.

We then introduce the network structure of the DNNs used for approximating f_i. A natural choice for the input layer is to use both $\mathbf{p}_i^o$, $\mathbf{p}_i$. However, inspired by Theorem 1 and the fact that (41) is computed consecutively, i.e. $\hat{\boldsymbol{\mu}}_i^{t-1}$ is generated after adding perturbations to $\mathbf{p}_i^{o,t-2}$ of the previous iteration that produced $\hat{\boldsymbol{\mu}}_i^{t-2}$, we propose to approximate the following mapping instead

$$\Delta\hat{\boldsymbol{\mu}}_i^{t-1} \leftarrow g_i\left(\mathbf{p}_i^{'} = [\Delta\mathbf{p}_i^{o,t-1}, \mathbf{p}_i^{o,t-2}, \mathbf{p}_i]\right) \tag{67}$$

$$\text{s.t. } \hat{\boldsymbol{\mu}}_i^{t-1} = \Delta\hat{\boldsymbol{\mu}}_i^{t-1} + \hat{\boldsymbol{\mu}}_i^{t-2}, \tag{68}$$

where $\Delta\mathbf{p}_i^{o,t-1} = \mathbf{p}_i^{o,t-1} - \mathbf{p}_i^{o,t-2}$. Since g_i only outputs the difference, the exact value of $\hat{\boldsymbol{\mu}}_i^{t=0}$ at the first iteration of Algorithm 1 should be computed via Algorithm 2. The DNNs work as nonlinear regressors $\hat{g}_i(\mathbf{p}_i^{'}; \boldsymbol{\theta}_i) \approx g_i(\mathbf{p}_i^{'})$, where $\boldsymbol{\theta}_i$ contains parameters for DNN. Note that $\hat{g}_i$ needs to be trained for every one of node $i = 1, \cdots, I$ due to our choice of the parameterization. This significantly increases the manual

labor in the process of network training. On the positive side, compared to more general type of parameterization, our choice requires lower generalization capacity from the DNNs.

The hidden layers are set as fully connected ones, with ReLU function $\mathrm{ReLU}(a) = \max(0, a)$ as the activation functions. At the output layer, we choose to generate the prediction of one entry of $\Delta\hat{\boldsymbol{\mu}}_i^t$, i.e.

$$\Delta\hat{\boldsymbol{\mu}}_i^t|_j \leftarrow \hat{g}_{i,j}(\mathbf{p}_i^{'}; \boldsymbol{\theta}_i, \pi_{i,j}), \text{ for } j = 1, \cdots, n_i, \tag{69}$$

where $\pi_{i,j}$ is the classification policy, according to which $\Delta\hat{\boldsymbol{\mu}}_i^t|_j$ is mapped into discreet classes. At each node, a total of n_i networks are requested to predict the entire $\Delta\hat{\boldsymbol{\mu}}_i^t$. We use Softmax function to process the output of the DNN. The DNN works as a multinomial classfier or a Softmax Regression classifier, predicting the class with the highest estimated probability.

From Assumption 1, the approximation error is related to $\hat{\boldsymbol{\mu}}_i^{t-1}$. However, at iteration t, $\hat{\boldsymbol{\mu}}_i^{t-1}$ is not yet available. We turn to integrate the DNN with the prior information from $\hat{\boldsymbol{\mu}}_i^{t-2}$, due to the correlation between $\hat{\boldsymbol{\mu}}_i^{t-2}$ and $\hat{\boldsymbol{\mu}}_i^{t-1}$, in the following heuristic manner

$$\Delta\hat{\boldsymbol{\mu}}_i^{t-1}|_j \leftarrow \begin{cases} \hat{g}_{i,j}(\mathbf{p}_i^{'}; \boldsymbol{\theta}_i, \pi_{i,j}^1) & \hat{\boldsymbol{\mu}}_i^{t-2}|_j \le c_{i,j}, \\ \hat{g}_{i,j}(\mathbf{p}_i^{'}; \boldsymbol{\theta}_i, \pi_{i,j}^2) & \hat{\boldsymbol{\mu}}_i^{t-2}|_j > c_{i,j}. \end{cases} \tag{70}$$

In Fig. 2, an example is provided where the 4^{th} entry of

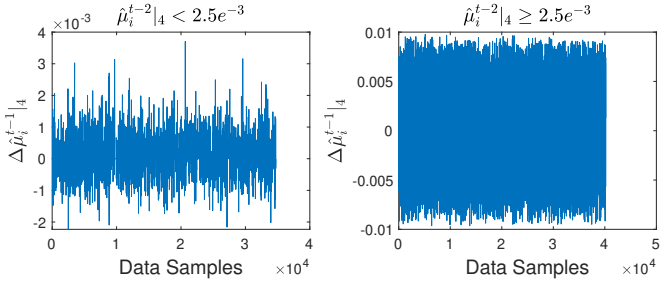

Fig. 2. Classifications of different granularity are related to the prior information on $\hat{\boldsymbol{\mu}}_i^{t-2}$.

$\Delta\hat{\boldsymbol{\mu}}_i^{t-1}$ has been shown to vary with significantly different ranges as $\hat{\boldsymbol{\mu}}_i^{t-2}|_4$ takes ranges of different values, suggesting that when $\hat{\boldsymbol{\mu}}_i^{t-2} < 2.5e-3$, a finer classification on $\Delta\hat{\boldsymbol{\mu}}_i^{t-1}$ can be used to reduce the approximation error. The major procedures for the generation of the training data are summarized as follows:

1) Generate data samples of the problem parameters $\mathbf{p}_i^{'} = [\Delta\mathbf{p}_i^{o,t-1}, \mathbf{p}_i^{o,t-1}, \mathbf{p}_i]$. The QoS bounds $\log(1+\gamma_{i,1})$ are set to be sampled from $\{0.25, 0.5, 0.75, 1\}$ (bit/s/Hz). The LOS channel matrix $\mathbf{H}_{i,j}^t$ is sampled at a rate of 1 second among a period of $\Delta t \approx 43s$, with rain attenuation factor ξs sampled from $\{0, -2.5, -5\}$ (dB). Denote the feasible set for $\mathbf{p}_i$ as $\mathcal{D}$. Samples set $\mathcal{D}$ according to the even distribution. For each $\mathbf{p}_i$, implement Algorithm 1 with its subproblem (41) solved through Algorithm 2, during which the parameter samples for $\Delta\mathbf{p}_i^{o,t-1}, \mathbf{p}_i^{o,t-1}$ are obtained.
2) To ascertain the label for each $\mathbf{p}_i^{'}$, the corresponding solution $\hat{\boldsymbol{\mu}}_i^t$ is first obtained by solving (41) through standard convex optimization algorithms, such as Algorithm 2. Based on the prior knowledge about the relationship between $\hat{\boldsymbol{\mu}}_i^{t-2}|_j$ and $\Delta\hat{\boldsymbol{\mu}}_i^{t-1}|_j$, such as the presented in (70), $\Delta\hat{\boldsymbol{\mu}}_i^{t-1} = \hat{\boldsymbol{\mu}}_i^{t-1} - \hat{\boldsymbol{\mu}}_i^{t-2}$ will then be classified into a total of 33 classes.

IV. Numerical Simulations

In this section, performance comparisons are provided between various beamforming schemes for heterogeneous multi-antenna LEO satellite networks, demonstrating the benefits from solving the original QoS based optimization problem (12). In the second part, numerical experiments covering key features of the proposed distributed algorithms, such as the convergence property, and the computational complexity will be given.

A. Superposition Coding based Beamforming for Heterogeneous Multi-user LEO Satellite Networks

The network geometry, such as the altitude and number of satellites per plane, is set according to the plan adopted in the Starlink project [2]. The major parameters for the simulations are given in Table I. As seen in Fig. 3, we focus

TABLE I
Major Simulation Parameters

Parameters	Values
Satellites per Plane	66
Altitude	550 km
Ka-band carrier frequency	30 GHz
Rician factor	$10\log(\kappa) = 10$ dB
Satellite Array Antenna Configuration	[23]
Terrestrial Receiver Antenna	8×8 rectangular array antenna
Number of pairs of users I	1080
Penalty para. for Lagrangian term ρ	1
Interference threshold for (16), (17) η	0.001
Combining para. in (44) τ	1/3

on a portion of the entire global network, which consists of three satellites $\mathrm{SAT}_1, \mathrm{SAT}_2, \mathrm{SAT}_3$ in the same orbit with the time-invariant pre-planned analog beamforming patterns $\bar{\mathbf{W}}^t = \bar{\mathbf{W}}$. We assume each satellite is equipped with at least two phased array antennas prescribed in Table I (or two collocated satellites, each equipped with one antenna). Every adjacent 121 subarrays of the satellite are put into one group, within which the subarrays point towards the same direction. Six analogue beams $\mathbf{W}_{i,j}, j = 1, \cdots, 6$ per satellite are generated to cover the neighboring area. The distance between the adjacent analogue beams is around 300 km.

We investigate a period of $\Delta t \approx 43$s, during which the satellites fly over and provide service to a terrestrial area within $250\mathrm{km} \le x \le 1500\mathrm{km}, 250\mathrm{km} \le y \le 750\mathrm{km}$, as shown in Fig. 3. The area is under a complete coverage over the period of Δt. Suppose the stronger terminals, $t_{i,2}$ are distributed uniformly within the area, with a minimum distance of 20 km. Terminal $t_{i,2}$ is paired with a weaker terminal $t_{i,1}$, that uniformly distributed around $t_{i,1}$ with a maximum distance of 10 km. Suppose that $\sigma_{i,1}/\sigma_{i,2} = 4$, due to for example larger antenna aperture at $t_{i,2}$.

In Fig. 4, we compare the performance of various types of beamforming schemes with that achieved by the optimal

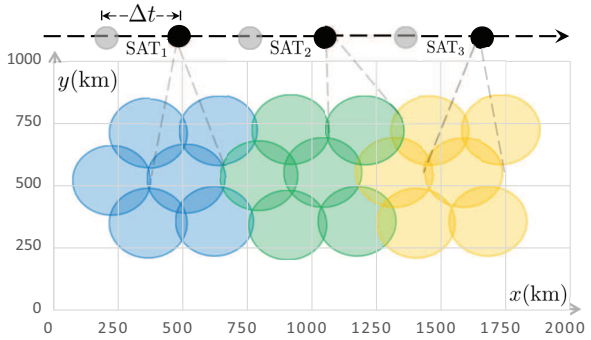

Fig. 3. Satellite topology with the pre-planned analog beam pattern.

solution to (12), which is denoted as Superposition Coding Beamforming (SCBF). The QoS requirement by the stronger user, i.e. $r_{i,2}$, is assumed to be twice as large as that for the weaker user $r_{i,1}$. Fig. 4 presents the total transmission power achieved using different schemes under a range of QoS requirements. OPBF_TDMA represents optimal beamforming combined with time division multiplexing (TDM), i.e. where $t_{i,1}, i = 1, \cdots I$ and $t_{i,2}, i = 1, \cdots I$ are put into 2 groups, each served in different time frames. Users within the same group are applied with the optimal linear beamforming [36]. Likewise, ZFBF_TDM denotes zero forcing beamforming combined with TDM. The time sharing coefficient τ_{ts} means that $1/\tau_{\text{ts}}$ of the time is for the transmission to $t_{i,1}$. SC_ZFBF is a low-complexity heuristic solution to (12) where only one digital beam is allocated to each user pair, i.e. the stronger and the weaker users' signals are superimposed within the same digital beam. The digital beams in SC_ZFBF are orthogonal to each other. The SCBF_ZFBF represents the scheme proposed in [17] that the channels are first diagonalized by applying zero-forcing beamforming across the paired users and the SCBF technique is then applied to only $t_{i,1}, t_{i,2}$. Note that SCBF_ZFBF and ZFBF_TDM perform poorly when

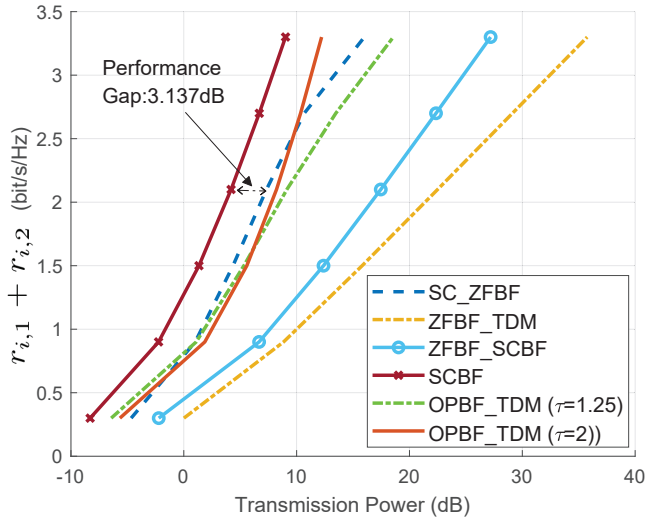

Fig. 4. Performance comparison between various beamforming schemes, $r_{i,2} = 2r_{i,1}$ for all i, $t = \Delta t/2$.

compared to others, due to the fact that the ZFBF operations in these two schemes are inefficient in dealing with the inter user interference. SCBF achieves superior performance with around a 3dB gain on average over the sub-optimal solution. The spectrum efficiency versus the transmission power curve stays almost unchanged during the period of Δt, demonstrating that while the satellites move rapidly, the QoS can be maintained with a stable power budget.

Notice that with the chosen spatial distribution of the terrestrial terminals, each analogue beam in average transmits to a total of 60 pairs of users simultaneously. Due to the power limited nature of the broadband satellite communication, in practice the operating point for LEO satellites with a massive array antenna is most likely around points with lower SE, such as 1 or 2 bit/s/Hz which combined with the multiplexing gain creates a total of 60-120 bit/s/Hz for each analog beam.

B. Computation Reduction through Decentralized Algorithms and Convex Optimization Approximation methods

To approximate (41), we train 2 types of DNNs for each pair of users with two different network scales. While the dimensions of the input $\mathbf{p}_i$ vary with different i, for each type of DNNs, we use a uniform structure of hidden layer and output layer that contains enough generalization capacity: for DNN 1, $512 \times 264 \times 132^4 \times 66^4 \times 33$ (11 layers including the output layers) and for DNN 2, $264 \times 132^4 \times 66^4 \times 33$ (10 layers). For the training of each individual DNN, the high-level API, Keras, is used for training and testing the DNNs based upon a dataset of 50,000 sampling points. DNN 1 requires around 2

TABLE II
DNN RELATED PARAMETERS

Parameters	DNN 1	DNN 2
Number of layers	12	11
Regularization coefficient	0.05e-3	0.1e-3
Number of multiplications	$M_1 = 246{,}246$	$M_2 = 111{,}078$
Approximation error $\epsilon_{i,1}$	$\epsilon_{i,1} < 0.25$	$\epsilon_{i,1} < 0.31$
Approximation error ϵ_2	$\epsilon_2 < 0.12$	$\epsilon_2 < 0.2$

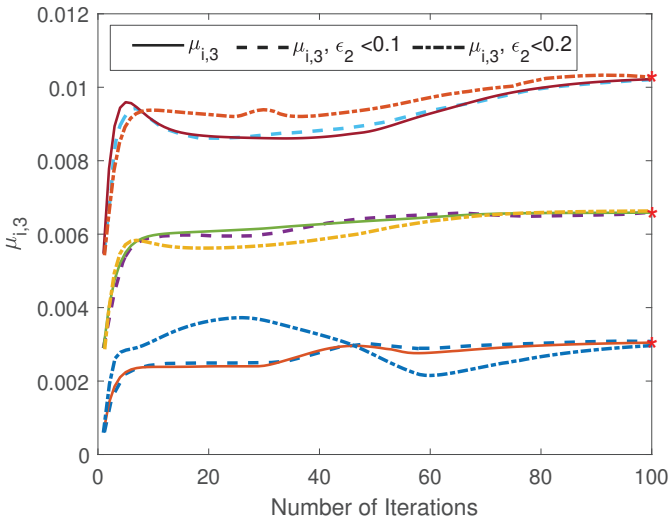

Fig. 5. Convergence of implementing Algorithm 2 with the solution of (41) approximated by DNNs.

times more multiplication operations than DNN 2 and achieves better approximation accuracy, which is characterized in Table II through different upper bounds on $\epsilon_{i,1}$ and ϵ_2, which are

related to the two types of approximation error defined in (53) and (54). Note that according to Theorem 1, the convergence for the algorithm is guaranteed with the implementation of either DNN 1 or DNN 2, since for either DNN 1 or DNN 2, the conditions required in Theorem 1 for the convergence, i.e. $c_1 = \rho(1-\tau-\epsilon_{i,1}^2/\tau) > 0, c_2 = \rho(\tau-2\tau^2-2c)-\rho^2\epsilon_2^2/\tau > 0$, are strictly satisfied.

To solve the dual problem (27), the respective per iteration complexity for the centralized solver, i.e. the interior-point method, the exact solving of Algorithm 1 with (41) solved by Alg. 2, as well as the two approximated version is given in Table III, where m_i is the number of iterations requested in the inner loop of Algorithm 2. In the case of our experimental setting, $n = 3I = 3240$ and in average $n_{i,j} = 26, n_i = 55, m_i = 195$, both Algorithm 1 and the approximated versions have an order of magnitude less per iteration complexity than the centralized algorithm. It should be noted that the per iteration complexity improvement provided by using DNNs comes at the expense of high computational cost involved in training a total number of I DNNs. Changes made to the analog beamforming pattern $\hat{\mathbf{W}}$ or to the terrestrial terminals, such as locations and parameters of antennas, would lead to a need for retraining corresponding DNNs.

TABLE III
PER ITERATION COMPLEXITY COMPARISON

Algorithms	per Iteration Complexity
Interior-point method	$n^2\sum_i^I(n_{i,1}^2+n_{i,2}^2)$
Alg. 1 with (41) solved by Alg. 2	$\sum_i^I m_i(n_{i,1}+n_{i,2})^4$
Alg. 1 with DNN 1	$M_1\sum_i^I n_i$
Alg. 1 with DNN 2	$M_2\sum_i^I n_i$

We next investigate the number of iterations for convergence requested by the centralized and the decentralized algorithms respectively. The number of iterations required in the interior-point method is bounded by $O((\sum_i^I(n_{i,1}+n_{i,2}))^{0.5})$ [26]. To show the convergence property of Algorithm 1 and its approximated versions, in Fig. 5, we present how $\mu_{i,3}$s converge within less than 100 iterations (3 dual variables $\mu_{i,3}$s are shown due to the space limitation). The solid line is the exact implementation of Algorithm 1 with (41) solved by Algorithm 2 exactly. The other two are generated respectively by Algorithm 1 with DNN 1 and DNN 2 approximating the solutions to (41). Recall that from Proposition 1, the sum of the dual variables equals to the objective value of the original problem, i.e. the total transmission power. Therefore from Fig. 5 it can be seen that the small differences between the optimal dual variables obtained from the centralized method (denoted with the asterisks) and those from the distributed algorithms ensure the latter schemes would have negligible performance degradation in contrast to the centralized optimal solution. From experimental results with the network setup in Table I, Algorithm 1 on average needs 2 to 3 times more iterations for convergence than the centralized interior-point method. Since the per iteration complexity of the latter is over 100 times higher, the overall complexity of Algorithm 1 is much lower than that requested by the centralized method. Algorithm 1 can further be speed up by up to I times through parallel computing processor, such as GPU Nvidia GTX 680, which has 1536 cores running at 1 GHz, and is evaluated in [32] as an efficient way of boosting the onboard processing power.

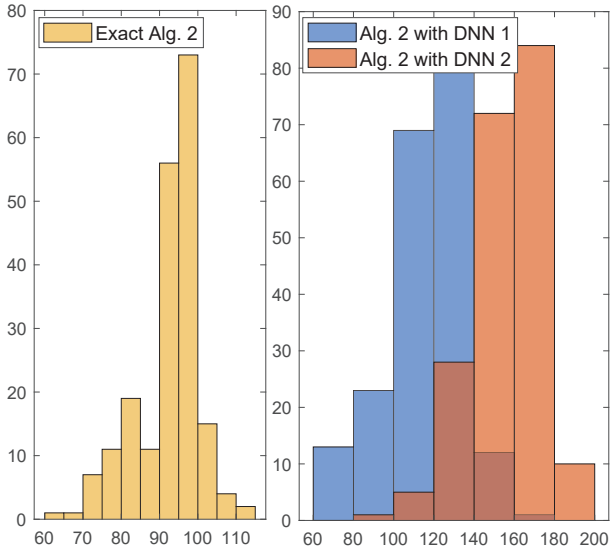

Fig. 6. Distribution of the number of iterations for convergence requested by Algorithm 1 and its approximated versions.

Finally, we analyze the complexity reduction offered by using DNNs to approximate the subproblem (41) in Algorithm 1. By traversing different network realizations (obtained via generating the QoS thresholds $\boldsymbol{\gamma}$ as well as the locations of terrestrial receivers randomly), the average number of iterations for convergence is obtained. Fig. 6 shows the histogram of the number of iterations for convergence, based on implementations of the three decentralized algorithms in 200 different network realizations. Compared to the exact running of Algorithm 1, the ones with DNN approximations use around 50 more iterations to converge. The extra iterations are compensated for by the much lower per iteration complexity of the DNN based methods. By using DNN 2, which produces a less accurate approximation than DNN 1, around 40 more iterations are needed, which is again a fair trade since DNN 2 has only half the multiplications in DNN 1.

V. CONCLUSIONS

Focused on the downlink transmissions from multiple LEO satellites to a massive number of heterogeneous terrestrial receivers, this paper studies beamforming algorithms in order to exploit the multiplexing gain as well as the array gain endowed by M-MIMO. To cater for the difference between the receiving capability of the IoT devices and the conventional wireless terminals, we pairs the heterogeneous receivers and combine transmit beamforming with superposition coding. The corresponding QoS constrained beamforming optimization is solved with novel distributed algorithms combined with deep learning techniques. The results show that our proposed method can improve the throughput performance (around 3 dB gain at the tested operational points) compared to other candidate schemes. At the same time w.r.t the centralized interior-point algorithm, we can reduce the overall computa-

tional complexity and speed up processing dramatically by using parallel computations.

APPENDIX A
PROOF OF PROPOSITION 1

Based on the technique used in [17], with certain fixed phase rotations $\{\phi_i\}$ we can construct the convex optimization problem (71), such that the solution set of it includes the optimal solution to the original problem (12).

$$\min_{\mathbf{D}} \sum_{i=1}^{I} \left(\|\mathbf{d}_{i,1}\|^2 + \|\mathbf{d}_{i,2}\|^2\right) \tag{71}$$

$$\text{s.t. } \gamma_{i,1}^{-0.5}|\widetilde{\mathbf{h}}_{i,1}^{\mathrm{H}}\mathbf{d}_{i,1}| \geq \left\| \begin{matrix} \widetilde{\mathbf{h}}_{i,1}^{\mathrm{H}}\mathbf{D}_{i,1} \\ \sigma_{i,1} \end{matrix} \right\|, \tag{72}$$

$$\gamma_{i,1}^{-0.5}|\widetilde{\mathbf{h}}_{i,2}^{\mathrm{H}}\mathbf{d}_{i,1}e^{j\phi_i}| \geq \left\| \begin{matrix} \widetilde{\mathbf{h}}_{i,2}^{\mathrm{H}}\mathbf{D}_{i,2} \\ \sigma_{i,2} \end{matrix} \right\|, \tag{73}$$

$$\gamma_{i,2}^{-0.5}|\widetilde{\mathbf{h}}_{i,2}^{\mathrm{H}}\mathbf{d}_{i,2}| \geq \left\| \begin{matrix} \widetilde{\mathbf{h}}_{i,2}^{\mathrm{H}}\mathbf{D}_{i,3} \\ \sigma_{i,2}, \end{matrix} \right\|, \text{for } i = 1, \cdots, I, \tag{74}$$

where $\|\widetilde{\mathbf{h}}_{i,1}^{\mathrm{H}}\mathbf{D}_{i,1}\|^2 = \zeta_{i,1} + \|\widetilde{\mathbf{h}}_{i,1}^{\mathrm{H}}\mathbf{d}_{i,2}\|^2$, $\|\widetilde{\mathbf{h}}_{i,2}^{\mathrm{H}}\mathbf{D}_{i,2}\|^2 = \zeta_{i,2} + \|\widetilde{\mathbf{h}}_{i,2}^{\mathrm{H}}\mathbf{d}_{i,2}\|^2$, $\|\widetilde{\mathbf{h}}_{i,2}^{\mathrm{H}}\mathbf{D}_{i,3}\|^2 = \zeta_{i,2}$. Problem (71) is convex since both of its objective function and constraints are convex. Strong duality therefore holds for (71), meaning the dual problem of (71) has the same optimal value as (71) or zero duality gap.

We then prove that the dual problem of the convex problem (71) is identical with that of the original problem (12), which completes the proof of the strong duality for problem (12). Introduce a set of strictly positive scalars such as

$$s_{i,1} = \gamma_{i,1}^{-0.5}|\widetilde{\mathbf{h}}_{i,1}^{\mathrm{H}}\mathbf{d}_{i,1}| + \left\| \begin{matrix} \widetilde{\mathbf{h}}_{i,1}^{\mathrm{H}}\mathbf{D}_{i,1} \\ \sigma_{i,1} \end{matrix} \right\|, \tag{75}$$

$$s_{i,2} = \gamma_{i,1}^{-0.5}|\widetilde{\mathbf{h}}_{i,2}^{\mathrm{H}}\mathbf{d}_{i,1}e^{j\phi_i}| + \left\| \begin{matrix} \widetilde{\mathbf{h}}_{i,2}^{\mathrm{H}}\mathbf{D}_{i,2} \\ \sigma_{i,2} \end{matrix} \right\|, \tag{76}$$

$$s_{i,3} = \gamma_{i,2}^{-0.5}|\widetilde{\mathbf{h}}_{i,2}^{\mathrm{H}}\mathbf{d}_{i,2}| + \left\| \begin{matrix} \widetilde{\mathbf{h}}_{i,2}^{\mathrm{H}}\mathbf{D}_{i,3} \\ \sigma_{i,2}, \end{matrix} \right\|, \text{for } i = 1, \cdots, I. \tag{77}$$

With the scalars introduced above, the Lagrangian for problem (71) can be written as

$$\begin{aligned} \mathcal{L}_{\mathrm{c}} = \sum_{i=1}^{I} \Big\{ & \|\mathbf{d}_{i,1}\|^2 + \|\mathbf{d}_{i,2}\|^2 + \frac{q_{i,1}}{s_{i,1}} \left(\gamma_{i,1}^{-1}|\widetilde{\mathbf{h}}_{i,1}^{\mathrm{H}}\mathbf{d}_{i,1}|^2 \right. \\ & \left. - \left(|\widetilde{\mathbf{h}}_{i,1}^{\mathrm{H}}\mathbf{D}_{i,1}|^2 + \sigma_{i,1}^2\right)\right) + \frac{q_{i,2}}{s_{i,2}} \left(\gamma_{i,1}^{-1}|\widetilde{\mathbf{h}}_{i,2}^{\mathrm{H}}\mathbf{d}_{i,1}|^2 \right. \\ & \left. - \left(|\widetilde{\mathbf{h}}_{i,2}^{\mathrm{H}}\mathbf{D}_{i,2}|^2 + \sigma_{i,2}^2\right)\right) + \frac{q_{i,3}}{s_{i,3}} \left(\gamma_{i,2}^{-1}|\widetilde{\mathbf{h}}_{i,2}^{\mathrm{H}}\mathbf{d}_{i,2}|^2 \right. \\ & \left. - \left(|\widetilde{\mathbf{h}}_{i,2}^{\mathrm{H}}\mathbf{D}_{i,3}|^2 + \sigma_{i,2}^2\right)\right) \Big\}. \end{aligned} \tag{78}$$

Since $s_{i,j} > 0, j = 1, 2, 3$, we can substitute $q_{i,j}/s_{i,j}$ with $\mu_{i,j} > 0$ in (78), showing that the two lagrangian functions, (24) and (78), are essentially the same. Therefore the dual problem for (12) and the dual problem for (71) are identical with each other.

APPENDIX B
FINDING THE PRIMAL OPTIMAL POINT FROM THE OPTIMAL DUAL VARIABLES

Based on Proposition 1, the KKT point for (12) is the optimal solution. We can derive the optimal primal variables $\mathbf{d}_{\mathbf{i,1}}^*, \mathbf{d}_{\mathbf{i,2}}^*$ from the KKT optimality condition. From the stationarity condition for Lagrangian function:

$$\begin{aligned} \mathbf{d}_{i,1}^* = & \left[\mathbf{I} + \sum_{j\in\mathcal{N}_c(i)} \mu_{j,1}\tilde{\mathbf{h}}_{i,1}\tilde{\mathbf{h}}_{i,1}^{\mathrm{H}} + \right. \\ & \left. \sum_{j\in\mathcal{M}_c(i)} (\mu_{j,2} + \mu_{j,3})\tilde{\mathbf{h}}_{i,2}\tilde{\mathbf{h}}_{i,2}^{\mathrm{H}})\right]^{-1} \frac{1}{\gamma_{i,1}} \left(\sum_{k=1}^{2} \mu_{i,k}\tilde{\mathbf{h}}_{i,k}\tilde{\mathbf{h}}_{i,k}^{\mathrm{H}}\right) \mathbf{d}_{i,1}^*, \\ = & \mathbf{A}_i\mathbf{d}_{i,1}^*, \end{aligned} \tag{79}$$

$$\begin{aligned} \mathbf{d}_{i,2}^* = & \left[\mathbf{I} + \sum_{j\in\mathcal{N}_c^s(i)} \mu_{j,1}\tilde{\mathbf{h}}_{i,1}\tilde{\mathbf{h}}_{i,1}^{\mathrm{H}} + \right. \\ & \left. \sum_{j\in\mathcal{M}_c^s(i)} (\mu_{j,2} + \mu_{j,3})\tilde{\mathbf{h}}_{i,2}\tilde{\mathbf{h}}_{i,2}^{\mathrm{H}} + \mu_{i,1}\tilde{\mathbf{h}}_{i,1}\tilde{\mathbf{h}}_{i,1}^{\mathrm{H}} + \mu_{i,2}\tilde{\mathbf{h}}_{i,2}\tilde{\mathbf{h}}_{i,2}^{\mathrm{H}}\right]^{-1} \\ & \frac{\mu_{i,3}}{\gamma_{i,2}}\tilde{\mathbf{h}}_{i,2}\tilde{\mathbf{h}}_{i,2}^{\mathrm{H}}\mathbf{d}_{i,2}^* = \mathbf{B}_i\tilde{\mathbf{h}}_{i,2}(\tilde{\mathbf{h}}_{i,2}^{\mathrm{H}}\mathbf{d}_{i,2}^*). \end{aligned} \tag{80}$$

Based on (79), $\mathbf{d}_{i,1}^*$ aligns with the eigenvector $\mathbf{v}_{i,1}$ of $\mathbf{A}_i$ corresponds to eigenvalue 1, i.e.,

$$\mathbf{d}_{i,1}^* = x_{i,1}\mathbf{v}_{i,1}, \tag{81}$$

where $x_{i,1}$ is the scalar waiting to be ascertained. Similarly from (80), $\mathbf{d}_{i,2}^*$ can be written as

$$\mathbf{d}_{i,2}^* = x_{i,2}\mathbf{v}_{i,2}, \tag{82}$$

where $\mathbf{v}_{i,2} = \mathbf{B}_i\tilde{\mathbf{h}}_{i,2}$. Substituting (81), (82) in the primal feasibility conditions (13) and (14), the systems equations on $x_{i,1}, x_{i,2}$ can be obtained.

APPENDIX C
PROOF OF PROPOSITION 2

$\partial\mathcal{P}(\boldsymbol{\gamma})$ is identical with the sub-gradient of $v(\mathbf{u})$ at point $\mathbf{u} = 0$, which is the optimal value function for the perturbed beamforming optimization problem (71) (adding small perturbation $\mathbf{u}$ to γ). The perturbed second-order conic constraints (72), (73) and (74) can be represented in the form of

$$G(\mathbf{d}, \mathbf{u}) \in \mathcal{K}, \tag{83}$$

where G maps $\mathbf{d}, \mathbf{u}$ to $\mathcal{K}$, which is the closed second-order cone. Take (72) as an example,

$$G_{i,1}(\mathbf{d}, u_{i,1}) = \begin{bmatrix} (\gamma_{i,1} + u_{i,1})^{-0.5}|\widetilde{\mathbf{h}}_{i,1}^{\mathrm{H}}\mathbf{d}_{i,1}| \\ \widetilde{\mathbf{h}}_{i,1}^{\mathrm{H}}\mathbf{D}_{i,1} \end{bmatrix}. \tag{84}$$

From Theorem 4.2 in [37], as long as the constraint qualification *Slater* condition is met, i.e. there exists $\bar{\mathbf{d}}$ such that

$$G(\bar{\mathbf{d}}, \mathbf{u} = 0) \in \mathrm{int}(\mathcal{K}), \tag{85}$$

$\partial v(0)$ can be obtained through the optimal dual variables. In our case, since all the channels are independent of each other, there always exist feasible solution such that (72), (73) and (74) are strictly satisfied,thus (85) is met.

REFERENCES

[1] OneWeb Non-Geostationary Satellite System (Attachment A), Federal Communications Commissions, Washington, DC, USA, 2016.

[2] SpaceX Non-Geostationary Satellite System (Attachment A), Federal Communications Commissions, Washington, DC, USA, 2016.

[3] M. Alzenad, M. Z. Shakir, H. Yanikomeroglu and M. Alouini, "FSO-Based Vertical Backhaul/Fronthaul Framework for 5G+ Wireless Networks," *IEEE Commun. Mag.*, vol. 56, no. 1, pp. 218-224, Jan. 2018.

[4] Handley Mark, "Delay is not an option: Low latency routing in space," in *Proc. of the 17th ACM Workshop on Hot Topics in Networks*, New York, USA, Nov. 2018, pp. 85–91.

[5] W. Liao, M. Hong, H. Farmanbar, X. Li, Z. Luo and H. Zhang, "Min Flow Rate Maximization for Software Defined Radio Access Networks," *IEEE J. Sel. Areas Commun.*, vol. 32, no. 6, pp. 1282-1294, June 2014.

[6] B. Di, L. Song, Y. Li and H. V. Poor, "Ultra-Dense LEO: Integration of Satellite Access Networks into 5G and Beyond," *IEEE Wireless Commun.*, vol. 26, no. 2, pp. 62-69, April 2019.

[7] M. Giordani and M. Zorzi, "Satellite Communication at Millimeter Waves: a Key Enabler of the 6G Era," in *2020 International Conference on Computing, Networking and Communications (ICNC)*, Big Island, HI, USA, 2020, pp. 383-388.

[8] L. You, K. -X. Li, J. Wang, X. Gao, X. -G. Xia and B. Ottersten, "Massive MIMO Transmission for LEO Satellite Communications," *IEEE J. Sel. Areas Commun.*, vol. 38, no. 8, pp. 1851-1865, Aug. 2020.

[9] L. You, K. Li, J. Wang, X. Gao, X. Xia and B. Ottersten, "LEO Satellite Communications with Massive MIMO," *ICC 2020 - 2020 IEEE International Conference on Communications (ICC)*, 2020, pp. 1-6.

[10] S. Kota , G. Giambene, "Satellite 5G: IoT use case for rural areas applications", in *Proc. of the Eleventh International Conference on Advances in Satellite and Space Communications (SPACOMM)*, Mar. 2019, pp. 24-28.

[11] N. Ahmed, D. De and I. Hussain, "Internet of Things (IoT) for Smart Precision Agriculture and Farming in Rural Areas," *IEEE Internet of Things J.*, vol. 5, no. 6, pp. 4890-4899, Dec. 2018.

[12] J. van't Hof, V. Karunanithi, *et al.*, "Low Latency IoT/M2M Using Nano-Satellites", in *Proc. 70th International Astronautical Congress (IAC)*, Washington DC, United States, Oct. 2019, pp. 21-25.

[13] M. De Sanctis, E. Cianca, G. Araniti, I. Bisio and R. Prasad, "Satellite Communications Supporting Internet of Remote Things," *IEEE Internet of Things J.*, vol. 3, no. 1, pp. 113-123, Feb. 2016.

[14] R. Deng, B. Di, S. Chen, S. Sun and L. Song, "Ultra-Dense LEO Satellite Offloading for Terrestrial Networks: How Much to Pay the Satellite Operator?," *IEEE Tran. Wireless Commun.*, vol. 19, no. 10, pp. 6240-6254, Oct. 2020.

[15] Chinchali, Sandeep, *et al.*, "Cellular network traffic scheduling with deep reinforcement learning.", in *Proc. Thirty-Second AAAI Conference on Artificial Intelligence*, April 2018, vol. 32, no. 1.

[16] M. Giordani, M. Polese, M. Mezzavilla, S. Rangan and M. Zorzi, "Toward 6G Networks: Use Cases and Technologies," *IEEE Commun. Mag.*, vol. 58, no. 3, pp. 55-61, Mar. 2020.

[17] X. Shi, J. S. Thompson, R. Liu, M. Safari and P. Cao, "Efficient Optimization Algorithms for Multi-User Beamforming With Superposition Coding," *IEEE Trans. on Commun.*, vol. 66, no. 12, pp. 5902-5915, Dec. 2018.

[18] Z. Chen, Z. Ding, X. Dai, and G. K. Karagiannidis, "On the application of quasi-degradation to MISO-NOMA downlink," *IEEE Trans. Signal Process.*, vol. 64, no. 23, pp. 6174–6189, Dec. 2016.

[19] Z. Xiao, L. Zhu, Z. Gao, D. O. Wu and X. Xia, "User Fairness Non-Orthogonal Multiple Access (NOMA) for Millimeter-Wave Communications With Analog Beamforming," *IEEE Trans. Wireless Commun.*, vol. 18, no. 7, pp. 3411-3423, July 2019.

[20] L. Dai, B. Wang, M. Peng and S. Chen, "Hybrid Precoding-Based Millimeter-Wave Massive MIMO-NOMA With Simultaneous Wireless Information and Power Transfer," *IEEE J. Sel. Areas Commun.*, vol. 37, no. 1, pp. 131-141, Jan. 2019.

[21] Z. Wei, L. Zhao, J. Guo, D. W. K. Ng and J. Yuan,"Multi-Beam NOMA for Hybrid mmWave Systems," *IEEE Trans. on Commun.*, vol. 67, no. 2, pp. 1705-1719, Feb. 2019.

[22] V. Mandawaria, E. Sharma and R. Budhiraja, "WSEE Maximization of mmWave NOMA Systems," *IEEE Commun, Letters*, vol. 23, no. 8, pp. 1413-1417, Aug. 2019.

[23] A. Ivanov, V. Teplyakov and V. Kalinin, "Mobile communication system with a hybrid phased array antenna system," *2015 IEEE East-West Design and Test Symposium (EWDTS)*, 2015, pp. 1-4.

[24] A. Ivanov, M. Stoliarenko, S. Kruglik, S. Novichkov and A. Savinov, "Dynamic Resource Allocation in LEO Satellite," in *2019 15th International Wireless Communications and Mobile Computing Conference (IWCMC)*, 2019, pp. 930-935.

[25] Ivanov, Andrey, et al. "Physical Layer Representation in LEO Satellite with a Hybrid Multi-Beamforming." 2019 15th International Wireless Communications Mobile Computing Conference (IWCMC). IEEE, 2019.

[26] S. Boyd and L. Vandenberghe, *Convex Optimization*, Cambridge, U.K.: Cambridge Univ. Press, 2004

[27] I. Notarnicola and G. Notarstefano, "Constraint-Coupled Distributed Optimization: A Relaxation and Duality Approach," *IEEE Trans. Control Network Systems*, vol. 7, no. 1, pp. 483-492, March 2020.

[28] A. Nedic and A. Ozdaglar, "Distributed Subgradient Methods for Multi-Agent Optimization," *IEEE Trans. Automatic Control*, vol. 54, no. 1, pp. 48-61, Jan. 2009.

[29] N. Matni, "Optimal zero-queue congestion control using ADMM," *2017 American Control Conference (ACC)*, 2017, pp. 5598-5604.

[30] N. Chatzipanagiotis and M. M. Zavlanos, "On the Convergence of a Distributed Augmented Lagrangian Method for Nonconvex Optimization," *IEEE Trans. Automatic Control*, vol. 62, no. 9, pp. 4405-4420, Sept. 2017.

[31] G. Furano, and M. Alessandra, "Roadmap for on-board processing and data handling systems in space." *Dependable Multicore Architectures at Nanoscale*, Springer, Cham, 2018, pp. 253-281.

[32] G. Lentaris, *et al.*, "High-performance embedded computing in space: Evaluation of platforms for vision-based navigation", *J. Aerospace Information Systems*, 2018, pp. 178-192.

[33] Ian Goodfellow, *et al.*, Deep learning, Book in preparation for MIT Press (www.deeplearningbook.org), 2016.

[34] M. Schubert and H. Boche, "Joint 'dirty paper' pre-coding and downlink beamforming," *IEEE Seventh International Symposium on Spread Spectrum Techniques and Applications*, 2002, pp. 536-540 vol.2.

[35] D. P. Palomar and Mung Chiang, "A tutorial on decomposition methods for network utility maximization," *IEEE J. Sel. Areas Commun.*, vol. 24, no. 8, pp. 1439-1451, Aug. 2006.

[36] E. Björnson, M. Bengtsson, and B. Ottersten, "Optimal multiuser transmit beamforming: A difficult problem with a simple solution structure," *IEEE Signal Process. Mag.*, vol. 31, no. 4, pp. 142–148, Jul. 2014.

[37] Bonnans, J. Frédéric, A. Shapiro. "Optimization problems with perturbations: A guided tour." SIAM review vol. 40, no. 2, 1998, pp. 228-264.

[38] K. I. Ahmed, H. Tabassum and E. Hossain, "Deep Learning for Radio Resource Allocation in Multi-Cell Networks," *IEEE Network*, vol. 33, no. 6, pp. 188-195, Nov.-Dec. 2019.

[39] C. Sun and C. Yang, "Learning to Optimize with Unsupervised Learning: Training Deep Neural Networks for URLLC," *2019 IEEE 30th Annual International Symposium on Personal, Indoor and Mobile Radio Communications (PIMRC)*, 2019, pp. 1-7.

[40] C. Sun, D. Liu and C. Yang, "Model-Free Unsupervised Learning for Optimization Problems with Constraints," *2019 25th Asia-Pacific Conference on Communications (APCC)*, 2019, pp. 392-397.

[41] N. Letzepis and A. J. Grant, "Capacity of the multiple spot beam satellite channel with rician fading," *IEEE Trans. Inf. Theory*, vol. 54, no. 11, pp. 5210–5222, Nov. 2008.

[42] Pelton, N. Joseph, S. Madry, and S. Camacho-Lara, eds. *Handbook of satellite applications*, New York: Springer, 2017.